NAVAL POSTGRADUATE SCHOOL

MONTEREY, CALIFORNIA

THESIS

LOW FREQUENCY ACOUSTIC INTENSITY PROPAGATION MODELING IN SHALLOW WATER WAVEGUIDES

by

Geoffrey R. Moss

June 2016

Thesis Co-Advisors: Kevin B. Smith
Thomas R. Howarth

THIS PAGE INTENTIONALLY LEFT BLANK

REPORT DOCUMENTATION PAGE			*Form Approved OMB No. 0704-0188*
Public reporting burden for this collection of information is estimated to average 1 hour per response, including the time for reviewing instruction, searching existing data sources, gathering and maintaining the data needed, and completing and reviewing the collection of information. Send comments regarding this burden estimate or any other aspect of this collection of information, including suggestions for reducing this burden, to Washington headquarters Services, Directorate for Information Operations and Reports, 1215 Jefferson Davis Highway, Suite 1204, Arlington, VA 22202-4302, and to the Office of Management and Budget, Paperwork Reduction Project (0704-0188) Washington, DC 20503.			
1. AGENCY USE ONLY ***(Leave blank)***	**2. REPORT DATE** June 2016	**3. REPORT TYPE AND DATES COVERED** Master's thesis	
4. TITLE AND SUBTITLE LOW FREQUENCY ACOUSTIC INTENSITY PROPAGATION MODELING IN SHALLOW WATER WAVEGUIDES			**5. FUNDING NUMBERS**
6. AUTHOR(S) Geoffrey R. Moss			
7. PERFORMING ORGANIZATION NAME(S) AND ADDRESS(ES) Naval Postgraduate School Monterey, CA 93943-5000			**8. PERFORMING ORGANIZATION REPORT NUMBER**
9. SPONSORING /MONITORING AGENCY NAME(S) AND ADDRESS(ES) N/A			**10. SPONSORING / MONITORING AGENCY REPORT NUMBER**
11. SUPPLEMENTARY NOTES The views expressed in this thesis are those of the author and do not reflect the official policy or position of the Department of Defense or the U.S. Government. IRB Protocol number ____N/A____.			
12a. DISTRIBUTION / AVAILABILITY STATEMENT Approved for public release; distribution is unlimited			**12b. DISTRIBUTION CODE** A

13. ABSTRACT (maximum 200 words)

Three popular numerical techniques are employed to examine the acoustic pressure and intensity features present in several environments of interest. Free field propagation and analytically tractable planar interfacial two-fluid transmission and reflection are used to benchmark the commercial software package COMSOL. Canonical Pekeris-type waveguides are used as initial points of comparison to illustrate COMSOL's ability to capture all pertinent physics. Additional environments with non-trivial bathymetry and varying sound speed profiles are then used to examine the rich feature set anticipated in experimental data. Predictions of recently estimated and experimentally verified physical phenomena serve as further proof of the accuracy of implementation of the Finite Element Method. Guidelines and recommendations are provided for future studies using COMSOL along with circumstances under which traditional treatment of the air-water interface is appropriate and when an explicit full-physics model is required.

14. SUBJECT TERMS wave propagation, normal modes, parabolic equation, finite element method, acoustic intensity, linear acoustics, PACS codes are: 43.20.-f general linear acoustics, 43.20.Mv waveguides, wave propagation in tubes and ducts, 43.30.Bp normal mode propagation of sound in water, 43.30.Gv backscattering, echoes, and reverberation in water due to combinations of boundaries			**15. NUMBER OF PAGES** 77
			16. PRICE CODE
17. SECURITY CLASSIFICATION OF REPORT Unclassified	**18. SECURITY CLASSIFICATION OF THIS PAGE** Unclassified	**19. SECURITY CLASSIFICATION OF ABSTRACT** Unclassified	**20. LIMITATION OF ABSTRACT** UU

NSN 7540-01-280-5500 Standard Form 298 (Rev. 2-89)
Prescribed by ANSI Std. 239-18

THIS PAGE INTENTIONALLY LEFT BLANK

Approved for public release; distribution is unlimited

LOW FREQUENCY ACOUSTIC INTENSITY PROPAGATION MODELING IN SHALLOW WATER WAVEGUIDES

Geoffrey R. Moss
Civilian, Department of the Navy
B.S.M.E, University of Massachusetts, Amherst, 2006
M.S.M.E., University of Massachusetts, Amherst, 2009

Submitted in partial fulfillment of the
requirements for the degree of

MASTER OF SCIENCE IN ENGINEERING ACOUSTICS

from the

NAVAL POSTGRADUATE SCHOOL
June 2016

Approved by: Kevin B. Smith
Thesis Co-Advisor

Thomas R. Howarth
Thesis Co-Advisor

Daphne Kapolka
Chair, Engineering Acoustics Academic Committee

THIS PAGE INTENTIONALLY LEFT BLANK

ABSTRACT

Three popular numerical techniques are employed to examine the acoustic pressure and intensity features present in several environments of interest. Free field propagation and analytically tractable planar interfacial two-fluid transmission and reflection are used to benchmark the commercial software package COMSOL. Canonical Pekeris-type waveguides are used as initial points of comparison to illustrate COMSOL's ability to capture all pertinent physics. Additional environments with non-trivial bathymetry and varying sound speed profiles are then used to examine the rich feature set anticipated in experimental data. Predictions of recently estimated and experimentally verified physical phenomena serve as further proof of the accuracy of implementation of the Finite Element Method. Guidelines and recommendations are provided for future studies using COMSOL along with circumstances under which traditional treatment of the air-water interface is appropriate and when an explicit full-physics model is required.

THIS PAGE INTENTIONALLY LEFT BLANK

TABLE OF CONTENTS

THIS PAGE INTENTIONALLY LEFT BLANK

LIST OF FIGURES

LIST OF ACRONYMS AND ABBREVIATIONS

DFT	Discrete Fourier Transform
FE	Finite Element
FEM	Finite Element Method
FFT	Fast Fourier Transform
FOAM	Finite Element Ocean Model
MMPE	Miami-Monterey Parabolic Equation
NM	Normal Modes
PE	Parabolic Equation
PML	Perfectly Matched Layer
SLFFT	Short Length Fast Fourier Transform
SOFAR	SOund Fixing And Ranging

THIS PAGE INTENTIONALLY LEFT BLANK

ACKNOWLEDGMENTS

The work presented in this thesis was supported by The Naval Undersea Warfare Center Division Newport (NUWCDIVNPT) and the Naval Postgraduate School via their distance learning program, and were it not for the time made available, completing both the coursework and research in the time allotted would have been impossible. Further, much of the side studies and verification were made possible by collaboration with senior subject-matter experts and external agencies. I would like to thank Drs. Kevin Smith, Ben Cray, Oleg Godin and Thomas Howarth, for their direction, guidance, and review of the material. In particular, investigation of the phenomenon of anomalous transparency led to significant contributions to this body of work. The major findings from that course of study were presented orally at the 22nd International Congress on Sound and Vibration, and published in the proceedings, with portions taken in whole or part and re-presented herein. Most notably, I wish to thank most sincerely Mr. Daniel Perez. He has been a mentor, colleague, friend, and confidant, volunteering hours of time in and outside of work to help with the non-trivial challenges faced when learning the nuances of acoustics and modeling.

THIS PAGE INTENTIONALLY LEFT BLANK

I. INTENSITY MODELING

A. HISTORICAL CONTEXT

The transmission of acoustic energy in waveguides has been a subject of study for many years. While a complete review of all progress to date is beyond the scope of this document, an excellent review of the modeling and simulation techniques available to the modern analyst is available commercially [1]. While numerous scenarios involve radiation of energy into a quiescent free field, there are similar problems in which energy generated by an acoustic source or scattered by a target becomes trapped by boundaries where the description of acoustic propagation is within the framework of guided waves. Examples of this scenario include interior sound transmission within the air ventilation ducts of buildings, certain speaker enclosures and most relevant to the work discussed herein, cases of underwater transmission. The boundaries acting to trap acoustic energy may come from the ocean's free surface, variations in the sound speed profile, and the bathymetry of the environment. For example, sound is trapped in the Sound Fixing And Ranging (SOFAR) channel due to fact that the sound speed decreases in the thermocline to a minimum at the SOFAR axis and then increases below. In this situation, the sound energy is successively "bent" upward and downward while it propagates, not directly interacting with a boundary.

When these are the governing circumstances of transmission, numerical ray tracing methods have historically been the analysis tool of choice. However, these numerical techniques are sensitive to initial conditions in range dependent environments [2], and such situations may necessitate a considerable number of deterministic trials to yield a statistically meaningful result. In cases where the sound wave interacts with a boundary, there is a predictable, but non-trivial change in both the magnitude and phase that needs to be computed accurately. When this interaction becomes part of the propagation path, ray methods may still be applicable, but can become cumbersome. To address this, there has been a large body of work devoted to analytical and numerical methods that correctly account for the transmission of energy within the bounded water column, as well as the interaction at the boundaries. For

brevity, an incomplete listing of techniques includes methods of Normal Modes (NM), Parabolic Equations (PE), the aforementioned ray tracing and the Finite Element Method (FEM). A summation of the pros and cons will be detailed in subsequent sections; however, it is worth noting that for the environments studied herein, the two most appropriate techniques are normal mode theory and the finite element method. It is worth noting that in strongly range dependent environments and at higher frequencies, the PE method may be more applicable and computationally efficient. While both techniques are applicable to a wide range of environments, their underlying assumptions and implementation limitations make them attractive for low frequency, range-dependent problems.

To date there have been several investigations into waveguides using normal mode theory, some even supplemented by finite element techniques, but there has been little direct comparison between the two methods for shallow water, low frequency propagation. The results of this study compare the output of a normal mode code, the output of a parabolic equation solver and the output from the commercial finite element software package COMSOL to examine the merits and detractors of each. It is noted that there is generally excellent agreement between the finite element method and normal mode theory, while there are discrepancies between their results and those predicted by the parabolic equation solver utilized here in some environments. These discrepancies are attributed to the assumptions behind each method and the specific implementation of the boundary condition necessary to define the problem.

B. BACKGROUND

Propagation of sound within a waveguide has received much attention, dating back to initial studies performed during the Second World War. The seminal paper in this field was arguably authored by Pekeris [3], who explored the acoustic pressure field present within a fluid medium above an infinite fluid half space. In the time since there have been many additions to his findings. Although a summary of additions to the field can be found in the classic text by Urick [4], a brief discussion of select recent contributions relevant to this particular study follows.

Kirby [5] studied the propagation of sound in a waveguide using a hybrid normal mode-finite element technique. His work employed a mode-matching scheme to couple the detailed results of a finite element calculation of the near field generated by an arbitrarily complicated body to a duct of constant cross section. Buckingham [6] examined the acoustic field in a Pekeris-type isospeed waveguide, including the effects of attenuation in the sediment layer over which the acoustic region is located. His work used numerically generated approximations for the natural mode shapes present within the water column. The results indicate that higher order; dissipative modes may still contribute to the measurable sound field when the sediment layer is of sufficiently high sound speed. Comparisons of normal mode techniques with experimental data taken in a laboratory setting were carried out by Schneiderwind [7]. This work showed that when the shear and compressional elastic behavior of the sediment layer are significant, a normal mode solution might be used as an accurate predictive tool at ranges far from the source.

The use of finite element techniques has gained traction in the past two decades due largely to the increase in computational resources available. Murphy [8] details the formulation and implementation of the Finite Element Ocean Model (FOAM), which, although unable to handle the effects of shear, presented several advantages over the normal mode and PE solutions at the time. Vendhan [9] coupled the finite element technique with a normal mode based solution at the terminating boundaries and compared his results of a range dependent waveguide with those of other numerical techniques.

Studies of acoustic intensity, a combination of both acoustic pressure and acoustic particle velocity, have become more common in recent years with advances in sensor technology and a renewed interest in the potential merits of directional sensing. Perhaps one of the most cited works in the field of acoustic intensity comes from Mann and Tichy [10]. Their work defines and explores the acoustic intensity field as not only a real component that describes energy flow, but also an imaginary component that describes energy storage within an acoustic medium. Smith [11] subsequently developed the general expressions required for computing the acoustic particle velocity field within the

framework of normal mode and parabolic equation methods in range-dependent environments.

More recently, Dall'Osto [12] examined the properties of the intensity field for a shallow water environment. This work compared measured data to the predictions of a numerical PE model for a 62m deep waveguide. They compute both the real (active) and imaginary (reactive) components of acoustic intensity. They then attribute the sign of the active intensity to the direction of propagating energy and are able to identify the direct and reflected contributions to the measured field. They note that the reactive intensity does not provide information on the direction of energy flux, but rather indicate where there are spatial gradients in the acoustic power field (square magnitude of pressure). Duan [13] presents a comparison of experimental data using two different methods of computing acoustic intensity for propagation in a waveguide. The authors examine the results of a hybrid theoretical-numerical dataset for a non-transient problem of propagation in a waveguide. The method used to generate theoretical predictions is complex, using a finite element approximation in the near field region immediately surrounding the source, to inform a normal mode expansion region in the propagating portion of the waveguide with eigen functions chosen to allow both forward and backward propagating waves similar to the prior work of Kirby [5]. Of note is that the experimental data to which they make comparisons was performed in air using a "p-u" type intensity probe (independent, collocated pressure and velocity sensors).

C. THEORY

The three major methods used to predict acoustic propagation within a shallow water waveguide at low frequencies are NM, PE, and FEM. The mathematical foundation of each method will be briefly reviewed, the coordinate systems will be defined and the output variable quantities to be compared will be reviewed.

The solution technique involving normal modes begins with the homogeneous, linear, inviscid wave equation neglecting any density contrasts at the water-sediment interface,

$$\nabla^2 p + k^2 p = 0, \qquad 1$$

where p is acoustic pressure and k is the acoustic wavenumber. In cylindrical coordinates, a mathematical solution is sought, assuming the pressure field may be represented as a separable solution (i.e., an expression comprised of the product of a functional form for range dependence and a functional form for depth dependence). For the purposes of comparison between methods, it is further assumed that there is no range dependence within the waveguide. With this simplification, the equation defining the normal modes of pressure oscillations within the waveguide is then given as

$$\frac{d^2\Psi_m(z)}{dz^2} = -\gamma_m^2(z)\Psi_m(z)\,, \qquad 2$$

where Ψ_m represents the eigenfunction, or mode shape for a given modal index, *m*, and γ_m is the quantized vertical component of propagating wavenumber.

A solution to the depth-separated equation is then sought by use of an eigenvalue solver in the presence of certain boundary conditions. For the ocean waveguide, two idealized boundary conditions corresponding to a rigid bottom and pressure release free surface may be easily realized. In the case of the pressure release surface ("acoustically soft" boundary), both the acoustic pressure and the mode shape take on a numerical value of zero, i.e.,

$$\Psi_{\mathrm{m}}(\mathrm{z} = 0) = 0. \qquad 3$$

In the case of an acoustically rigid bottom, the normal component of the acoustic particle velocity will be zero. This is implemented by enforcing the vertical derivative of the mode shape to approach zero at the depth of the waveguide, D, i.e.,

$$\frac{\partial \Psi_m}{\partial z}(z = D) = 0. \qquad 4$$

This solution technique ensures that each mode shape is unique, orthogonal and has real eigenvalues. As will be shown later, the ocean surface may be accurately modeled as a true pressure release boundary at which the pressure goes to zero when the

product of the source depth (distance from the free surface) and its excitation wavenumber, *k* are of order 0.1 or greater. The wavenumber, *k*, is defined as the ratio of the circular frequency (ω) of excitation to the sound speed (c) or

$$k = \frac{\omega}{c} = \frac{2\pi f}{c}. \qquad 5$$

For more general boundaries, such as those separating two media of contrasting materials, the boundary condition becomes more complicated. For example, the boundary condition that must be satisfied between a water layer, of sound speed c_w and density ρ_w, overlying a fluid bottom layer, of sound speed c_b and density ρ_b, takes the form

$$\Psi_{\mathrm{m}}(\mathrm{D}) + \frac{\rho_b}{\rho_w} \frac{1}{\sqrt{k^2 - \frac{\omega^2}{c_w^2} - \frac{\omega^2}{c_b^2}}} \frac{d\Psi_{\mathrm{m}}}{dz}(\mathrm{D}) = 0. \qquad 6$$

The introduction of this type of boundary condition creates several complex phenomena, as will be described in more detail later.

In contrast to the exact solution of an analytical technique to the differential equation describing the normal modes present within a waveguide, the FE Method seeks an approximate but convergent solution to partial differential equations subject to boundary conditions through the use of linear algebra and polynomial expansion. Solution to Equation (1) is sought by discretizing the problem domain into a series of smaller domains of finite size. These elements are connected to each other at nodes, and the value of the acoustic pressure at these nodes is determined by obtaining the coefficient values to a polynomial set of shape functions describing the variation of acoustic pressure between nodes. COMSOL allows for flexibility in the order of polynomial shape function and permits the user to choose first through fifth order.

Parabolic Equation methods also begin with the Helmholtz equation (Equation 1), but take a different approach towards solution. By introducing a "reduced" pressure field, $u(r,z,\phi)$, defined by $p(r,z,\phi) = \frac{1}{\sqrt{r}} u(r,z,\phi)$, and defining the operator notation $P_{op} = \frac{\partial}{\partial r}$

and $Q_{op} = \left(\mu + \varepsilon + \nu + 1\right)^{1/2}$, where $\varepsilon = n^2 - 1$, $\mu = \frac{1}{k_0^2}\frac{\partial^2}{\partial z^2}$, and $\nu = \frac{1}{k_0^2 r^2}\frac{\partial^2}{\partial \phi^2}$, the parabolic equation formulation takes the form

$$\left(P_{op}^2 + k_0^2 Q_{op}^2\right)u = 0. \qquad 7$$

Using an orthogonal cylindrical coordinate system, the radial, azimuthal and axial ordinates are represented with variables *r, z,* and φ, respectively. A reference acoustic wavenumber is defined as k_0 and the medium specific index of refraction is represented as *n*.

Assuming that acoustic energy primarily propagates outward (cylindrically divergent from the source point), the Helmholtz equation may be factored, leading to an equation of the parabolic form given by

$$P_{op}\Psi(r,z,\varphi) = \mathrm{i}k_0 Q_{op}\Psi(r,z,\varphi) \text{ or } -\frac{i}{k_0}\frac{\partial\Psi(r,z,\varphi)}{\partial r} = Q_{op}\Psi(r,z,\varphi). \qquad 8$$

Introducing a slowly modulating PE field function $\psi\left(r,z,\phi\right)$, such that $\Psi = \psi e^{ik_0 r}$, the pressure field may now be represented by

$$p(r,z,\varphi) = P_0\sqrt{\frac{R_0}{r}}\psi(r,z,\varphi)e^{ik_0 r}. \qquad 9$$

This form may be further simplified into differential operators acting on the PE field function, and the treatment of these operators is a field of active research [14]. However, for this course of study, the Monterey Miami Parabolic Equation (MMPE) formulation of Smith [15], which utilizes a split-step Fourier algorithm, was chosen as the representative implementation. Only the 2-D version is utilized, since 3-D effects are beyond the scope of this study. In addition, this form of the MMPE model utilized the Thomson-Chapman wide-angle approximation for the operator Q_{op} [16], and employs the traditional boundary smoothing functions associated with the split-step Fourier algorithm. The executable code used is available from the Ocean Acoustics Library [17].

It is worth noting that fundamentally both methods generate approximate solutions to the same governing Helmholtz equation (Equation 1). For normal mode theory used herein, the assumption of range independence is made explicitly. Although there are many other implementations of normal mode theory (manifest in codes, such as KRAKEN, COUPLE, MOATL, and others [17] that do allow for range dependence), the finite element method places no such restrictions on the computational space. It is also worth noting that the boundary conditions to be compared in the initial studies are ideal. The choice of pressure release at the free surface is not mandatory within the normal mode theory, but the relative impedance mismatch between air and water makes it convenient to implement and typically results in acceptable accuracy.

MMPE implements an image source method to address the free surface, consistent with an ideal pressure release boundary condition. While there are potentially some tricks that could be played to simulate the air-water interface explicitly, an ideal pressure release boundary is used in all MMPE runs. Similarly, within COMSOL the free surface may be specified as an ideal pressure release boundary, or coupled to another acoustic media in order to capture the effects of reflection from a free surface more accurately. Interaction with the bottom bathymetry is an area of active research, with many potential theorems available to address the complicated interaction between the acoustic fluid and elastic bottoms with varying degrees of stiffness. Application of boundary conditions appropriate to reflection from sandy, lossy sediment is possible within both methods, but for the purposes of comparison, initial studies employ an ideal acoustically rigid bottom. This choice precludes the use of MMPE for initial studies due to the implementation of a blending function necessary to model the water-sediment interaction. For a perfectly rigid boundary, the resulting impedance contrast approaches infinity and the MMPE output is entirely contaminated by this singularity. However, in later modeling efforts where the sediment is modeled as an acoustic media, all three methods are compared directly.

D. MODELING

The simplified environment initially studied was an ideal two-dimensional waveguide of constant bathymetry. The water column was chosen to be 100 m deep, with a 50 Hz continuous wave (CW) omnidirectional source placed at a depth of 75 m from the free surface. A constant 1500 m/s, sound speed profile in a range independent 1000 kg/m^3 density environment was used. In order to examine the effects of propagation, the waveguide was modeled out to a range of 500 times the depth of the water column, or 5000 m. In both methods, the 5000 m range modeled was assumed to extend outward towards infinity, an approximation enforced in different ways between the methods. In the first model, the bottom is assumed acoustically rigid, and in the second, it is a planar interface with a second acoustic media with sound speed of 1900 m/s and density of 1610 kg/m^3. The effects of shear are not included, and there is no attenuation in either acoustic media. A diagram of this setup is shown in Figure 1. Note that p = 0 represents a pressure release surface and v = 0 represents an acoustically rigid boundary at the bottom of the waveguide

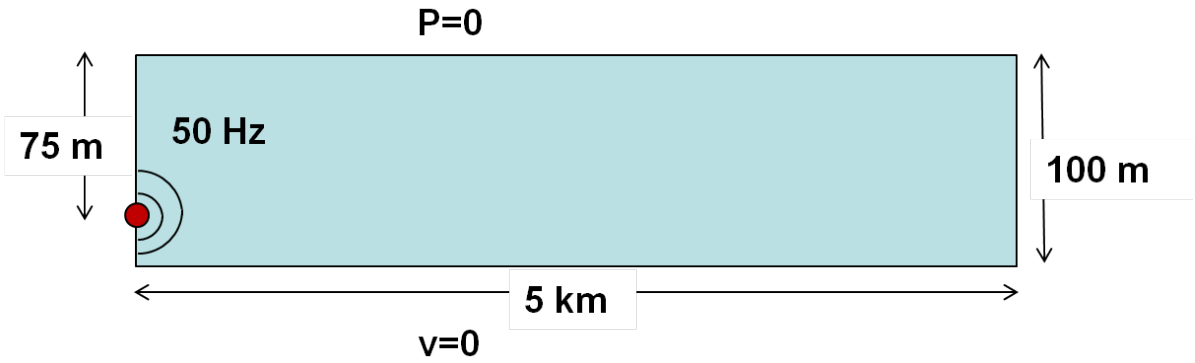

Figure 1. Diagram of Problem Setup (Not to Scale)

The accuracy of any finite element solution should be verified through a mesh convergence study, but heuristically it has been demonstrated that 8–10 linear elements or 6–8 quadratic elements per wavelength are sufficient to resolve propagating wave phenomenon [18]. While these resolution requirements are sufficient to recover the pressure field accurately, one aim of this study is also to examine the intensity field,

which requires accurate calculation of the particle velocity. Under conditions of CW excitation, the particle velocity vector is related to the harmonically varying scalar pressure field via spatial derivatives, i.e.,

$$v_i = \frac{1}{i\omega\rho}\frac{\partial P}{\partial x_i}. \qquad 10$$

In the finite element method, the velocity field is determined by taking spatial gradients in the direction of interest. The accurate recovery of gradients is strongly mesh dependent, and prior work has indicated that 10–20 quadratic elements per wavelength are required to recover smoothly varying spatial gradients [19]. Fortunately, in the 2D axisymmetric formulation, for shallow water, low frequency scenarios, this requirement still allows for a tractable problem size.

In the execution of the normal modes code, the potential for examining a non-rigid boundary was desired. As such, the formulation of Clay and Medwin [20] was coded into Matlab [21]. This formulation allows for the interaction of the water column with a second acoustic media with disparate density and sound speed. From a theoretical viewpoint, the number of modes present in a waveguide is dependent on not only the bounding geometry, but the boundary conditions as well. A thorough treatment of the mathematical techniques available for rigorous analysis is described by Brekhovskikh [22]. Assuming cylindrical spreading, this pressure field is the product of a radially propagating component k_{nr}, described by a Hankel function, and a vertical standing component k_{nz} with the total wavenumber given as the geometric mean of the two, i.e.,

$$k = \sqrt{k_{nr}^2 + k_{nz}^2}\,. \qquad 11$$

A brief review of the decomposition of the acoustic field present in a waveguide with ideal boundary conditions (rigid bottom, pressure release top) can be described as a summation over all modes that can fit an odd number of quarter wavelengths within the

height, *D*, of the waveguide. Mathematically this requires that

$$k_{nz} = (2n-1)\frac{\pi}{2D}, \qquad 12$$

where n is the modal index, and k_{nz} is the axial component of the acoustic wavenumber.

Note that because the total wavenumber is independent of geometry, there are modes for which the radial wavenumber component of propagation must become imaginary. When this occurs, the modes are said to be "evanescent." Accordingly, for a given geometry and frequency, there are finite number of modes, *N*, that will propagate out radially. This can be defined as

$$\mathrm{N} = \mathrm{mod}\left[\left(\frac{2fD}{c}\right) + \frac{1}{2}\right]. \qquad 13$$

Such modes are considered to be "trapped" because their energy propagates radially outward from the source at a real angle, confined by the boundaries and are subject only to geometric spreading and material/medium losses, without penetration into the other bounding media.

When the water column with sound speed c_1 sits atop a second sedimentary acoustic media with sound speed c_2, the lower boundary condition requires that both the pressure and particle velocities be continuous across the interface. Recall that the development of Transmission and Reflection coefficients for incident plane waves at a planar boundary require that the incident and reflected angles as measured from the interface must be equal. Although there are a number of interesting possibilities, with rigorous development and analysis available, [23] for the sake of brevity the applications of interest here are those where the water column has a slower sound speed. Under these circumstances the critical angle (θ_c) relative to the "grazing angle" is defined as

$$\theta_c = \cos^{-1}\frac{c_1}{c_2}. \qquad 14$$

For all incident angles of incidence greater than the critical angle there is transmitted energy propagating into the sediment and the lower refraction angle is real, representing the trapped modes, which decay in range as $\frac{1}{\sqrt{r}}$. For angles shallower than critical, there is no transmitted energy propagating into the bottom and the lower refraction angle becomes complex. At the critical angle, there is a singularity in the modal solution, which represents a boundary wave in the lower medium that propagates along the interface, decaying in range as $\frac{1}{r}$. This phenomenon will lead to several interesting effects as will be shown later.

Since both media are being excited at a single frequency, two unique total wavenumbers must exist, one in each media, e.g., $k_i = \frac{2\pi f}{c_i}$. The propagation vector within a given medium is still dependent on the geometry as indicated by Equations (11 and 12). Note however, the conditions of continuity also introduce the possibility of transmission of energy across the water-sediment interface, the magnitude of which decreases exponentially with range. More precisely, if a mode corresponds to conditions involving propagation angles steeper than the critical angle, defined by Equation (14), the boundary condition itself becomes a complex valued function, and the mode, while still propagating radially, decays exponentially in range. Under these circumstances, energy is propagating along the axis of the waveguide, but also into the sediment. Accordingly, energy in that mode is no longer "trapped" by the boundary of the waveguide, but said to be "leaky."

The number of trapped modes present for a given environment of depth *D* excited at frequency *f* with wave speeds in the water column and bottom, c_1 and c_2 , respectively, may be calculated as

$$\mathrm{N} = \mathrm{mod}\left[\left(\frac{2D}{c_1/f}\right)\sqrt{1-\frac{c_1^2}{c_2^2}}+\frac{1}{2}\right]. \qquad 15$$

Initial modeling attempted to mimic the effects of a rigid bottom by setting the values of sound speed and density in the second media to be several orders of magnitude larger than in the water column, numerically equal to 10^{20} for both. In this case, the second term

in the radicand approaches zero, Equation (15) approaches Equation (13) and the pressure field should be represented by only “trapped” and not “leaky” modes.

The pressure field excited by a mono frequency source is then the summation of the product of each trapped mode at all depths and the value of the mode at the source depth, i.e.,

$$\mathrm{p}(r,z) = \sum_{m=1}^{N_{trapped}} \frac{\Psi_m(z_s)\Psi_m e^{iK_m r}}{\sqrt{K_m}}, \qquad 16$$

where m is the modal index and z_s is the depth of the source.

Similarly, the velocity field components may be obtained by taking spatial derivatives of the pressure field, and scaling by the local impedance (here a constant value). The complex intensity field may then be simply computed by taking one-half the product of the pressure field and the complex conjugate of the particle velocity at each grid point, i.e.,

$$\mathrm{J} \equiv \frac{1}{2} p u^{*}, \qquad 17$$

where the * denotes complex conjugation.

In the simulation results presented here, a fixed grid with spacing of 1 m in the vertical direction and 1 m in the radial direction was used to generate smooth plots. Results are not presented for the sake of brevity, but through parametric variation of grid spacing, it was found that the results of the normal mode code were largely insensitive to output grid spacing for this environment.

Execution of the COMSOL model was carried out via the pressure acoustics interface within version 4.4. Unlike the other two methods where the source may be specified by a delta function, the pressure field in the absence of any boundaries may be defined a priori and the scattering interactions will be computed by the software. This method has several advantages, though the implementation should be handled carefully. Within the COMSOL framework, the formulation of the Helmholtz equation allows the

user to solve for either the "scattered" or "total" pressure fields. By definition, the scattered field is generated by interaction with boundaries and/or scattering bodies. The incident field is defined as the field, which would exist in the total absence of any boundaries or scattering bodies. The total field is the field that would be measured by an observer, and is defined as the sum of the scattered and incident fields. These definitions are mathematically viable since the governing differential equation is linear, and each field individually satisfies the governing equation. The sum of the individual solutions will itself be an admissible solution. The advantages of these definitions are twofold: first, it allows the analyst insight into the relative position of scattered features and the source of reflections, and second, it provides a natural separation of scales that allow for better conditioned numerics. In general structural acoustics problems for which the finite element method is typically employed, the incident acoustic field may be one or more orders of magnitude larger than the scattered field. Since the incident field is defined before any computations are carried out, only the scattered field need be modeled. In the case of propagation modeling, the field scattered from the boundaries is of the same order of magnitude as the incident field (except immediately near the source due to the $\frac{1}{r^2}$ decay), but can be treated within the same mathematical and numerical framework. In both cases, the total field may then be determined by summing the scattered field with the incident field. Implementation in COMSOL is somewhat cumbersome, requiring that the incident field be defined mathematically and added to the solution domain as a "background pressure field."

Although the nomenclature is somewhat misleading, the intent is to allow the software to compute accurately the relatively small-scattered component of the acoustic field. For the case of the monopole source, this is defined as

$$\mathrm{P}_{incident}(r,t) = \frac{1}{r} e^{-i(kr-\omega t)}, \qquad 18$$

where r is the radial ordinate, k is the free space acoustic wavenumber, and ω is the angular frequency of excitation.

Note that there is a $1/r$ decay in Equation (18) that results in a singularity at the acoustic center of the source. Finite element techniques cannot tolerate such a singularity within the computational domain, so a scheme for dealing with this issue is presented as follows. The cylindrical waveguide is set-up in the 2D axisymmetric mode of COMSOL. In this mode, only a single radial cross section of the waveguide need be modeled. This reduces the problem size down to a tractable "slice" of the physical domain, which may be recovered by revolving the computational domain about its axis. This, however, places a restriction that a point source must be placed at the axis of revolution. In order to remove the singularity from the computational domain, a circular portion of the grid, centered at the acoustic center of the point source was removed, and an absorbent boundary placed on the terminating faces of the resulting mesh. COMSOL has implemented several methods for absorbing waves, and the use of a "spherical wave radiation" condition has been shown to be excellent in these situations. A closer view of the segmented geometry with the boundary condition highlighted is shown in Figure 2.

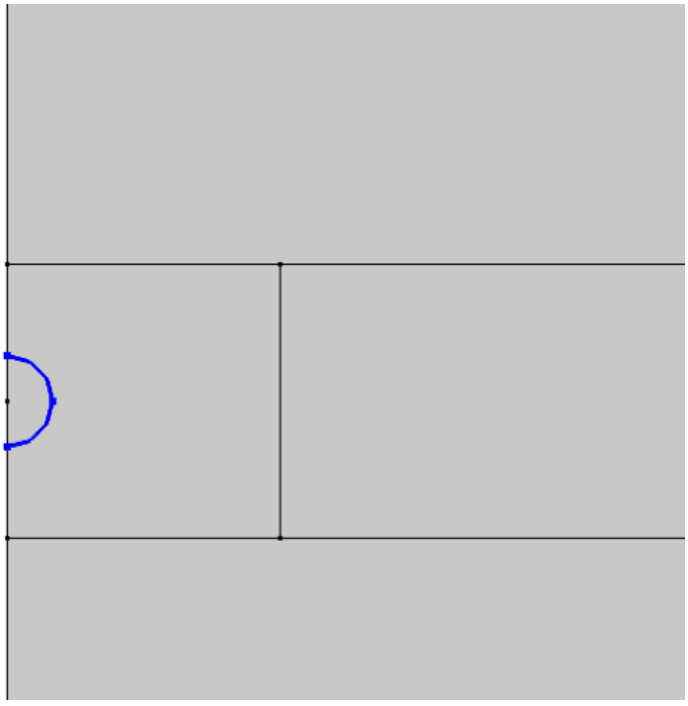

Figure 2. Close View of Segmented Geometry with Source Region and Absorbing Boundary Highlighted in Blue

In the case of the acoustically rigid bottom, only the water column must be explicitly modeled and meshed. At the surface interface, a Dirichlet-type boundary condition is enforced whereby the pressure is equal to zero. The bottom interface can be completely specified by a Neumann-type boundary condition whereby the normal derivative (related to the particle velocity) of the pressure field must go to zero. Note that because of the relation between pressure gradient and particle velocity, given by equation 10this is equivalent to enforcing that acoustic particle motion match the stationary boundary motion, a concept similar to the "no slip" boundary condition often employed in the field of fluid mechanics. The complete geometry is represented by Figure 1. In the case where the bottom is modeled as a second acoustic media, no boundary condition need be specified between the two domains; COMSOL automatically enforces continuity of pressure and velocity along the interface. A schematic of this situation is presented in Figure 3.

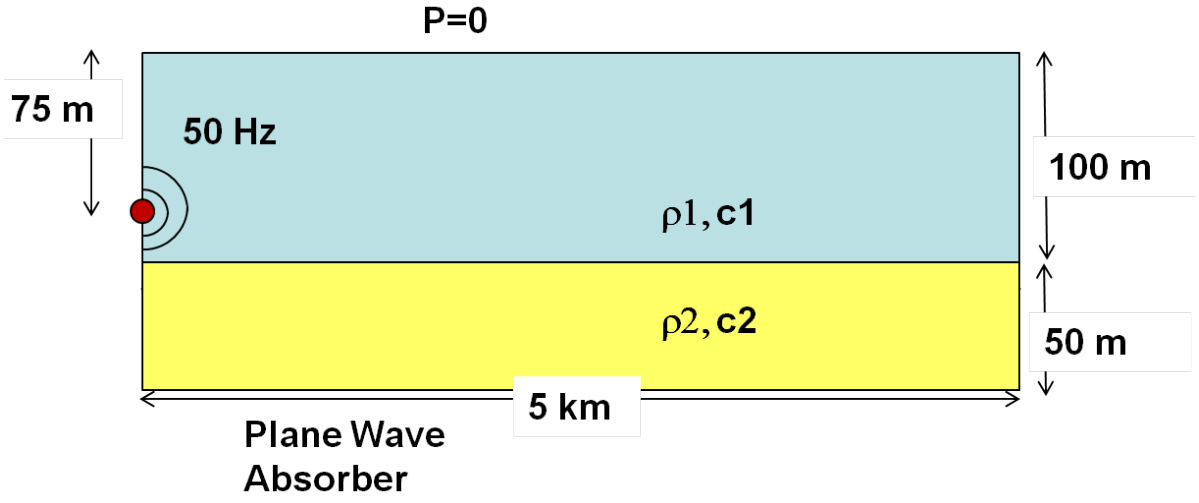

Figure 3. Diagram of Two Fluid Approximation (Not to Scale)

However, in order to capture the waves transmitted across and reflected by the interface, a background pressure field must be applied to the domain in which the source is active. As stated above, the background pressure field in the water column is known a priori and may be defined completely by a single frequency and wavenumber. For the case of the rigid bottom, where only a single sound speed is defined in the water column,

the choice of wavenumber is obvious. In the case where two acoustic media are present, there are two sound speeds and thus two potential choices of wavenumber. In the COMSOL framework, the interface between the two domains acts as a scattering boundary. Because the background field is defined as that which would be present in the absence of any scattering bodies, it is the wavenumber in the acoustic media in which the source is located that must be used to specify the incident field.

An alternate approach of modeling the incident field was explored wherein a spherical wetted surface is driven with constant radial acceleration. This methodology approximates a volumetric monopole source and obviates the need to define a background pressure field, and is consistent with historical theoretical treatments of monopole sources. A source wavenumber must still be specified and an additional caveat that should be noted: in order to enforce a surface acceleration such that a constant source level is obtained, the fluid properties and frequency of excitation must be taken into account. Because the acceleration required for a constant source level is dependent on both frequency and source size, an equation based acceleration, as given in [24],

$$\mathrm{a}(f, r, R) = \frac{2\pi f p(R)}{\rho_0 c_0}\left(\frac{1}{kr} + i\right), \tag{19}$$

is enforced at all points along the circular boundary defining the source volume.

The fluid properties (density, sound speed and wavenumber) are again referenced to the acoustic domain containing the source, f is the excitation frequency, r is the source radius and $p(R)$ is the pressure specified at some distance R. For the studies presented herein, a 0 deciBel (dB) ref 1 μPa @ 1m source level was desired, and the pressure at 1m from the acoustic center of the finite size source was held constant at 1 μPa. This methodology was implemented as a result of some anomalous findings and apparent discrepancies between the methods and is discussed in detail in section II, and specifically in Figure 21. The results are important because they allow for direct modeling of actual transduction devices. While the field of fully coupled fluid-elastic structural codes has been under development for many decades, and the demonstration of acceleration boundaries to generate near field results is not new, the promise of a fully,

directly coupled problem could yield new insight into the governing mechanisms of long range propagation and transducer design without the use of intermediary techniques, such as the Kirchoff-Helmholtz surface integration techniques.

The incident/scattered field separation approach has been verified by modeling a unit cell and enforcing Floquet-type [25] boundary conditions between the left and right terminating faces to mimic an infinitely wide domain. This problem is created in the COMSOL 2D plane strain physics module. In this model, the interface between the two media is modeled in the same way, and both the top and bottom boundaries are terminated with "planar wave radiation" conditions to prevent spurious reflections. Pointwise constraints are enforced between the left and right boundaries, separated by distance L, such that the horizontal component of the acoustic wave-vector remains continuous across the domain boundaries, e.g.

$$P_{right} = P_{left} e^{ik_x L}. \qquad 20$$

A diagram showing the two fluids, location of boundaries and left and right pressures is shown in Figure 4.

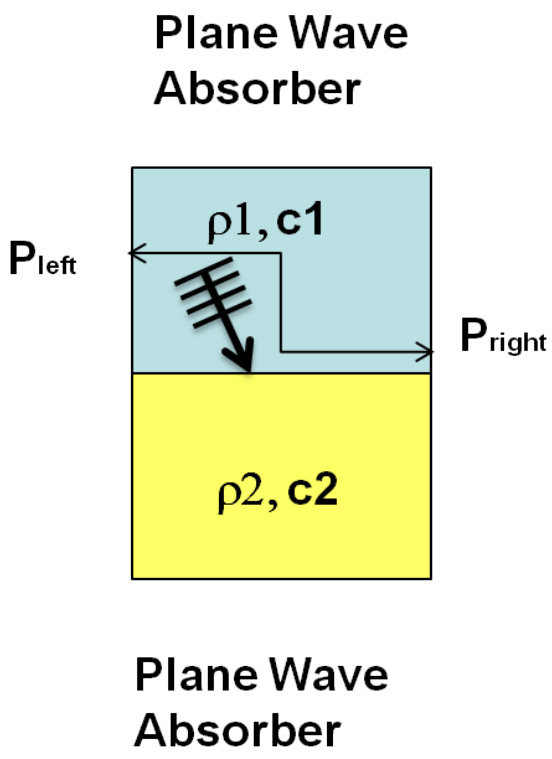

Figure 4. Diagram of Floquet Periodic Unit Cell

This cell is used to verify transmission and reflection between two fluid domains using the background pressure field paradigm.

Here again, the x component of the wavenumber used in the constraining equation is that of the water column. A background pressure field is defined in the source acoustic medium by incident plane waves propagating in the first fluid at some angle. In this case, the angles of incidence (θ_{in}) propagating in medium 1 and refraction (θ_{refra}) in medium 2 are governed by Snell's law of refraction using a coordinate system relative to normal incidence, mathematically stated as

$$\frac{\sin\theta_{in}}{c_1} = \frac{\sin\theta_{refra}}{c_2}. \qquad 21$$

This provides an analytic expression against which the COMSOL solution may be verified. A simple check on the validity of this method is performed using equal sound speeds and densities in the two acoustic media and observing that there is no reflection or refraction from the interface.

In applying boundary conditions to a finite computational domain modeling one that approaches an infinitely large space, there are several options available. The first is to apply an "impedance" boundary condition. Experimentation with this option has shown that it prevents most, but not all of the reflections at the far end of the domain. The two more accurate options available are the "radiation" conditions and the Perfectly Matched Layer (PML). The use of PML has been shown to be very effective at higher frequencies [26] but requires an additional domain to be meshed and several parameters to be specified. In contrast, the radiation boundary condition based on the second order Bayliss-Gunsberger-Turkel formulation [27], designed to permit only outgoing propagating waves has been shown to be more effective at lower frequencies. Accordingly, at the far end of the water column, a "cylindrical wave radiation" boundary condition is applied.

In addition to the Pekeris-type waveguide [3] with a planar boundary, several additional environments were studied, including deep water bathymetries with linear slopes converging to a constant shallow depth. This environment is nominally 600 m deep, with a section sloping upward to a depth of 150 m at a distance of 4500 m from the source, followed by a second upward slope to a depth of 100 m at a range of 5500 m from the source, finally ending in a planar waveguide of constant 100 m depth for an additional 5000 m as shown in Figure 5.

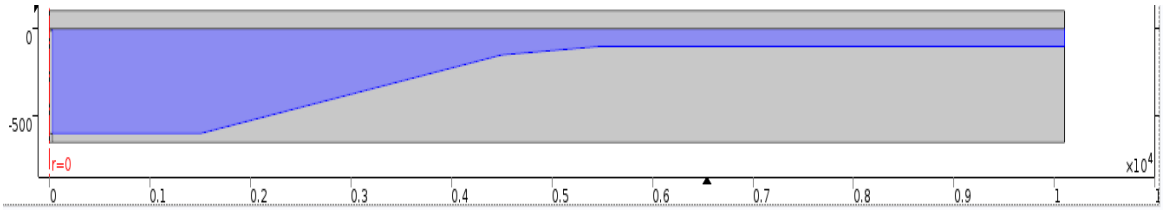

Figure 5. Schematic Representation of Up Sloping Bathymetry

An additional point of comparison between COMSOL and MMPE comes from a standard Pekeris waveguide [11]. For this study, the environment can be summarized as a 200 m water column with a constant sound speed of 1500 m/s, and density of 1000 kg/m^3 in contact with a planar sediment layer possessing a constant sound speed of 1700 m/s

and density of 1500 kg/m^3, excited by a 200 Hz monopole source located at a depth of 100 m. Both fluid media are considered lossless. Runtime parameters were provided by the author and execution of the MMPE code was carried out locally. A comparable COMSOL model was created and the transmission loss predicted by the two codes was compared.

During the course of modeling these environments, an additional point of comparison and interesting corner case was studied, wherein the air-water interface was not assumed a perfect reflector with known phase shift. Unlike the normal mode technique that enforces a pressure release boundary, or the parabolic equation technique, which implements an image source to model the air-water interface, COMSOL can be quickly configured to treat this two fluid boundary explicitly, capturing all of the underling physics. In order to explore the FE method's applicability in such circumstances, a model of a finite sized monopole source located in a semi-infinite half space of air and water contact was created. The source was allowed to translate vertically within the half-space, penetrating the interface such that the acoustic fields produced for a continuous wave discrete frequency excitation were available for study. The boundaries of the two half spaces were truncated with both absorbing boundaries and perfectly matched layers in order to compare the efficacy of modeling propagation from this source off to infinity. A schematic of the model half spaces is presented in Figure 6.

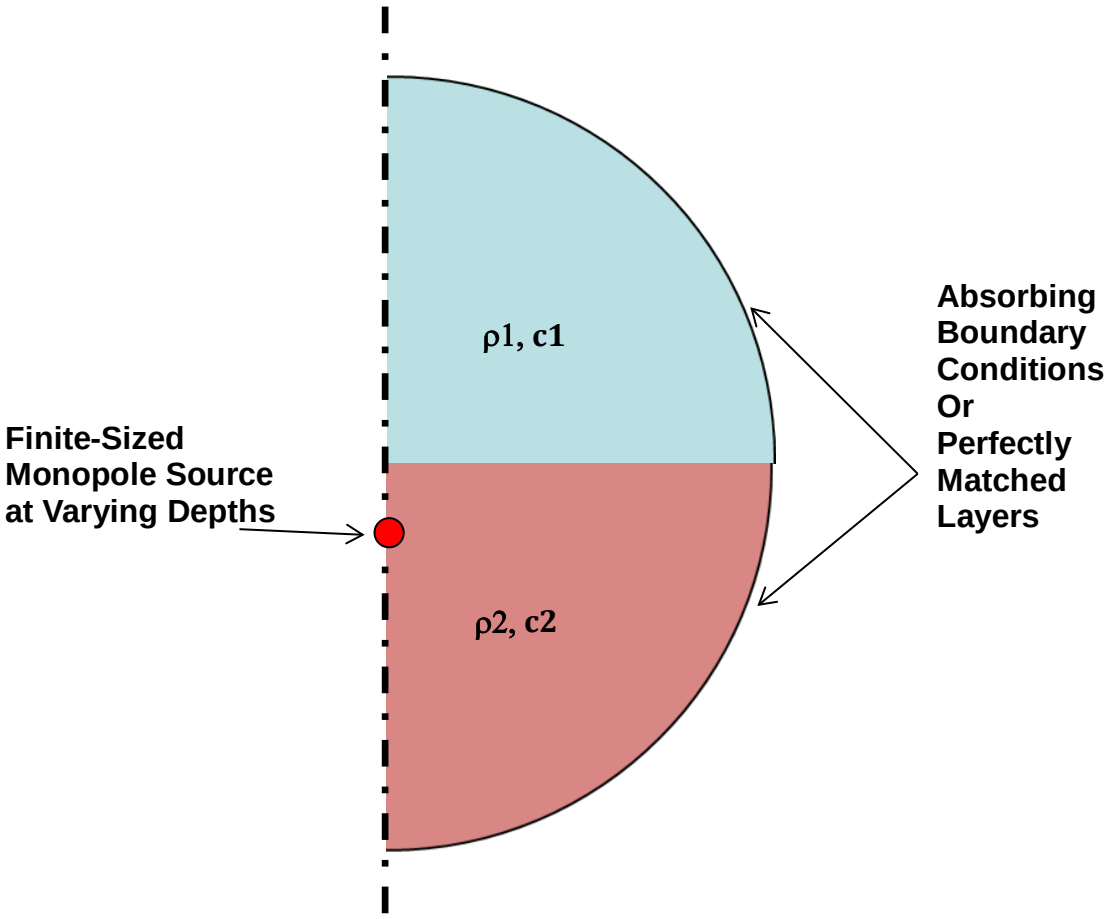

Figure 6. Axisymmetric Model of Two Semi-Infinite Half Spaces with Planar Air-Water Interface

II. RESULTS

A. IDEAL PEKERIS WAVEGUIDE

The first set of results comes from models of the ideal rigid bottom waveguide. Several relevant metrics may be used to compare the output of the two solution methodologies appropriate for this environment (finite element and normal modes). The first qualitative method is to examine color contour plots of the complex acoustic fields. Presented in Figure 7 are contour plots of the magnitude of the total acoustic field as predicted by COMSOL and the normal mode code.

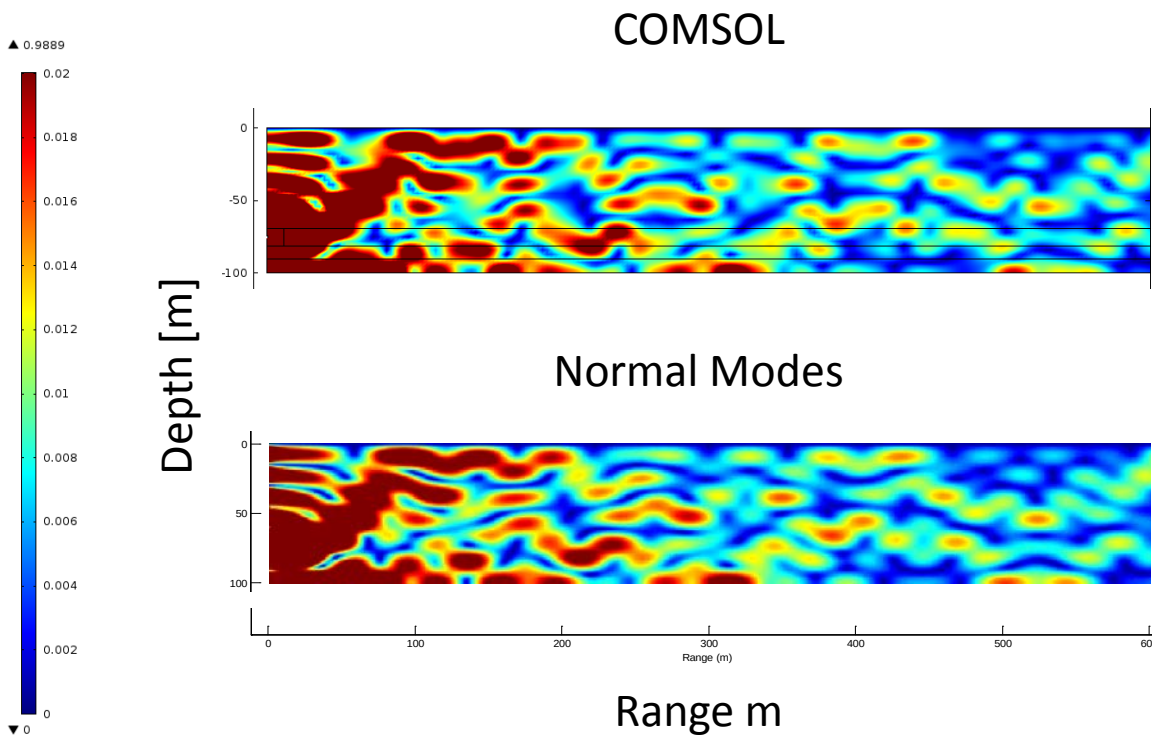

Figure 7. Comparison of COMSOL and Normal Modes: Acoustic Magnitude

Code predicted magnitude of acoustic pressure over the 0–600 m range from source.

It can be readily observed that there is excellent qualitative agreement between the two methods. There are some slight discrepancies in the location of peaks in the field,

but overall the features predicted by the two methods are congruent. Due to the formulation of the normal modes theory, and the approximations introduced by the spherical absorber placed around the source location, it is anticipated that the near field of both methods would show minor differences. A comparison is therefore made to the fields predicted by the two codes at longer ranges. In addition to the magnitude of the field, which serves to illustrate many features of the pressure field, one method to explore the differences in the two techniques is to examine variations in complex phase angle. Therefore, presented in Figure 8 are contour plots of the imaginary component of the total pressure field over a range of 2000 to 2800 m from the source location.

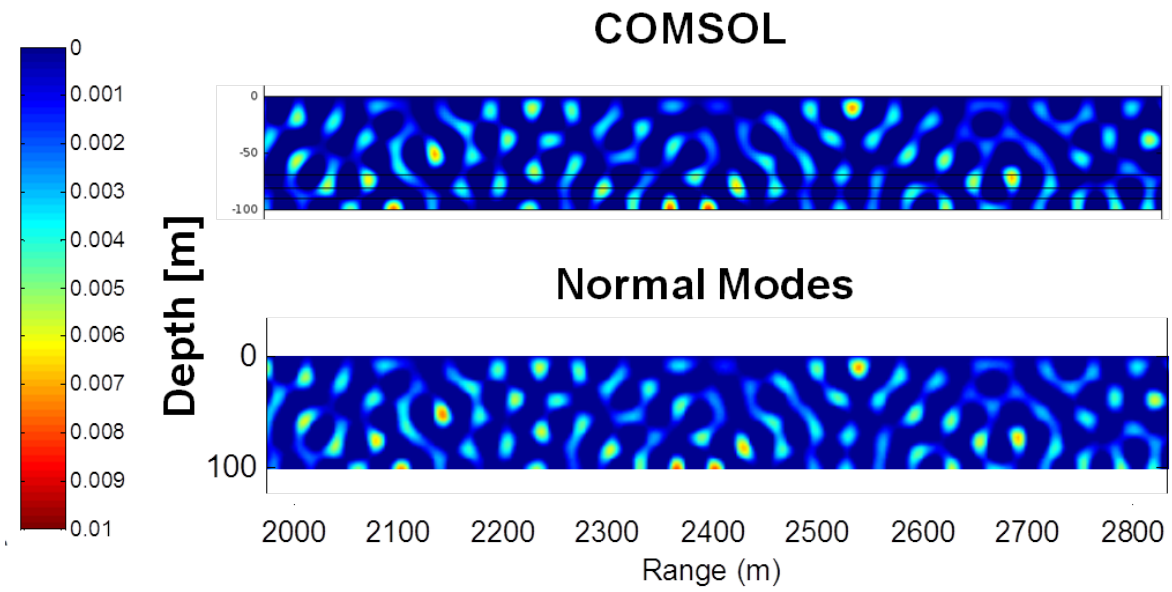

Figure 8. Comparison of COMSOL and Normal Modes: Imaginary Component

Code predicted imaginary component of the total acoustic pressure field over the 2000–2800 m range from source.

At these longer ranges, the agreement between the two codes is significantly better. There are clearly identifiable features present in both solutions. As an example, there is a pronounced area of relatively high magnitude at 2150 m in range and 50 m in depth, surrounded by a ring like set of intense points. The surrounding structure and magnitudes of the features in the pressure field has been predicted by both methods.

While potentially interesting to examine in detail, the acoustic particle velocity field is computed from spatial gradients in pressure. Because of the agreement in the pressure field, it is anticipated that the velocity fields would agree as well. Rather than illustrate this field directly and graphically, a comparison is made between the two codes of a derivative quantity, the acoustic intensity (J), as defined by Equation 17. For brevity and a better quantitative metric, single line plots of the active and reactive components of vertical intensity at a range of 4500 m are presented in Figure 9. The dotted red lines are produced by COMSOL, while the continuous blue curve is produced by normal mode theory. The leftmost images are the active (real) component of vertical intensity and the rightmost images are the reactive (imaginary) component.

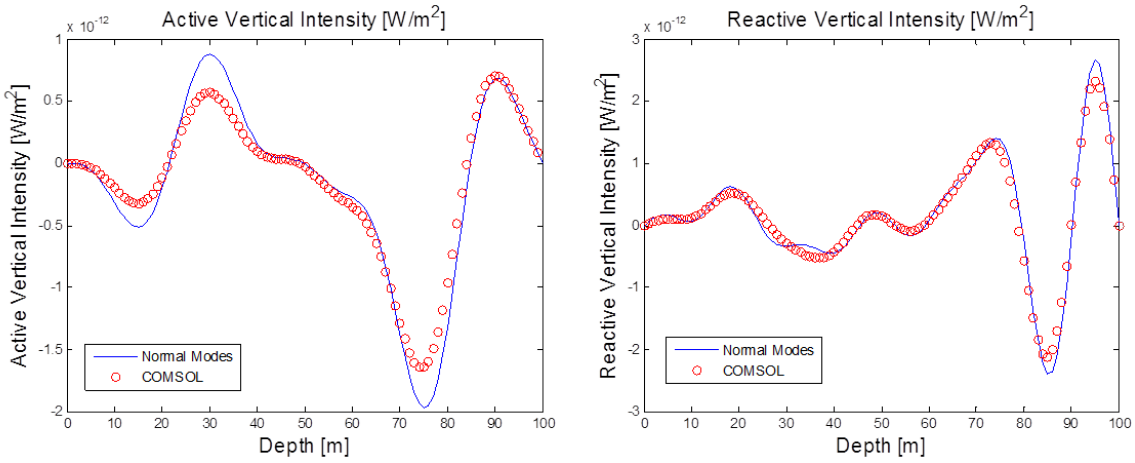

Figure 9. Line Plots of the Active Component of the Vertical Acoustic Intensity

Taken along the depth of the water column at a range of 4500 m from the source.

Examining the two plots, it is clear that there is excellent qualitative and quantitative agreement between the solutions predicted by the two methods. The shapes of the vertical intensity values are consistent, and the magnitudes predicted by both codes are in agreement. There are minor variations in the magnitude of the intensity peaks between the two methods, but the location of features and their values is consistent.

It was found that due to the assumption of a perfectly reflective bottom and the frequencies studied in the initial verification efforts, the MMPE model was inappropriate. Therefore, the results for this environment are not presented. However, when

environments that are more realistic are modeled, the MMPE technique produces high quality, computationally efficient predictions of the acoustic field. Given that the ultimate utility of any model is to predict the propagation of energy in realistic environments, and all three methods compared in this paper should, in theory, be capable of handling interactions with a second acoustic media, the results of the environment described in the modeling section are now presented for comparison.

The verification of the method of background pressure field and acceleration-type boundary is noteworthy for the two fluid domains because all pressure fields predicted for a waveguide are predicated on the ability of COMSOL to handle the interface and correctly predict several important phenomena. Once demonstrated that the method is correctly calculating the transmitted and reflected waves at this boundary, the results of a two fluid waveguide are presented.

B. FLOQUET UNIT CELL

Verification of the two fluid interaction is demonstrated by examining two specific results from the Floquet unit cell: harmonic plane waves incident on the fluid-fluid boundary at both the sub critical angle and super critical angle. In the case of subcritical incidence, the transmitted and reflected angles are both real and readily predicted by Snell's law as provided in Equation 21. In the case of the supercritical angle, the transmitted angle becomes imaginary and theory predicts transition from a transmitted wave to decaying evanescent wave. In this case, the amplitude of the transmitted wave decays exponentially away from the interface with the energy dissipating primarily along the boundary. For the wave speeds chosen in this illustrative example, 1500 and 1700 m/s, the critical angle is calculated as $\theta_c = 62$ degrees relative to vertical. Presented in Figure 10 are angles of incidence $\theta_{inc} = 36$ degrees and $\theta_{inc} = 66$ degrees. For the sub critical incidence of 36 degrees, theory predicts an angle of transmission of 42 degrees.

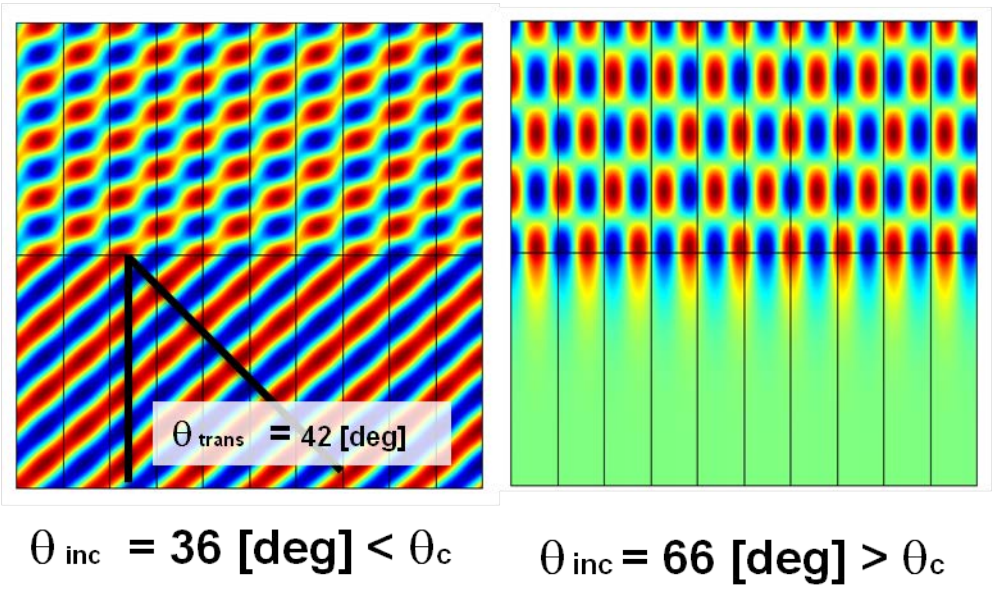

Figure 10. Pressure Field Generated by Scattering Off Fluid Interface

At two angles of incidence, one sub critical and one supercritical.

In the case of an angle of incidence of 36 degrees shown on the left of Figure 10, it can be seen that energy propagates into the second acoustic media, and by taking a measurement of the angle of transmission, it can be seen that the energy is indeed propagating at 42 degrees relative to normal. In the case of an angle of incidence of 66 degrees shown on the right of Figure 10, it can be seen that the energy decays exponentially away from the boundary, and does not propagate into the second fluid, but rather along the boundary. This also serves as verification of the method of implementing a background pressure field. This plot is also an excellent graphical means for illustrating evanescent wave propagation.

C. EXAMINATION OF HEAD WAVE

While the correct prediction of the evanescent field generated by interaction with a second acoustic media has been demonstrated, it is necessary to verify the propagation of the faster traveling wave in the lower media to all points in the domain. In order to show the effects of the fast moving, laterally traveling “head wave,” two visual aids are presented below. First, a time transient model was created and driven at a single continuous wave frequency. Such a model is not well suited to predicting steady state

phenomenon, but does provide clear visual evidence of the head wave. Following a similar procedure for MMPE execution, a schematic diagram of the water column, sediment layer and deep bottom later is shown in Figure 11. Note that the boundary conditions between the COMSOL model shown in Figure 3 and the MMPE model differ at the terminating bottom-most face. In the MMPE model, the deeper portion of the sediment layer contains a spatial filter that acts to remove the energy as it approaches the edge of the computational domain, whereas in the COMSOL model, a plane wave-absorbing boundary is used to prevent spurious reflections back to the computational domain pressure field.

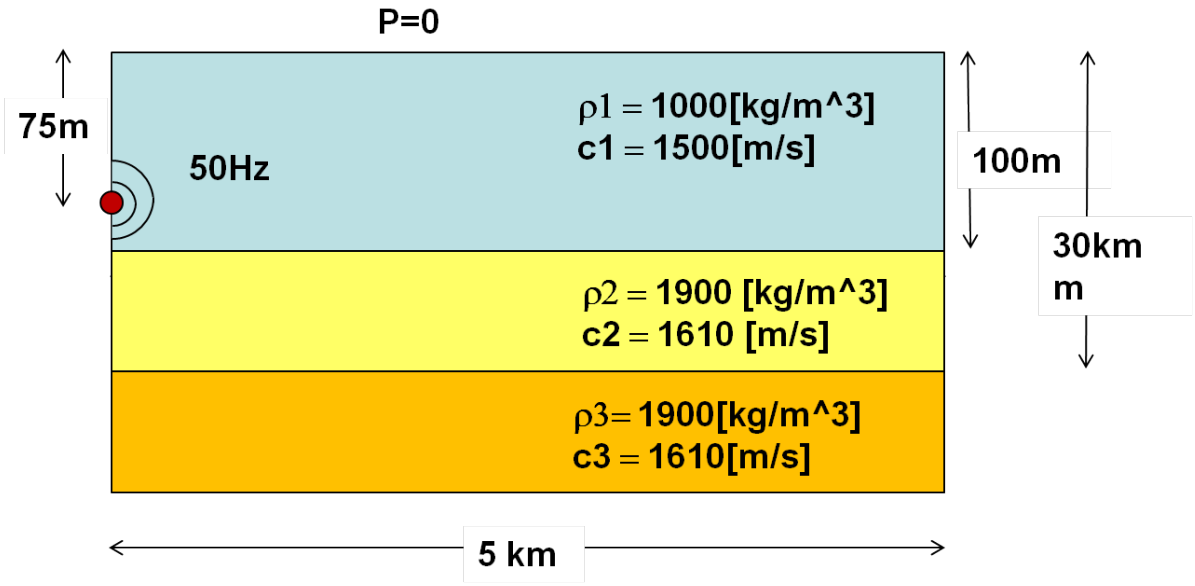

Figure 11. Diagram of the Sediment Bottom Environment Modeled in MMPE (Not to Scale)

The bathymetry shown in Figure 3 was used in the aforementioned time transient run. The sound speed in the second media was parametrically varied in order to observe the effects on the acoustic field generated in the water column. Presented in Figure 12 are color contour plots of the acoustic fields predicted by COMSOL for two disparate sediment sound speeds at the same point in simulation time. In the upper panel, the sediment sound speed is set equal to that of the water column and the early time, near field spherical spreading, prior to any reflections from boundaries, or energy becoming

trapped in the cylindrical section of the waveguide is readily apparent. Interference structure is observed as reflections from the free surface interact with the monopole source field. In the lower panel, the sediment sound speed is set to be four times that of the water column. Under such conditions, the same near field spherical spreading is observed. However, additional interference structure can be seen in the near field since both bottom and free surface reflections interact with the monopole source. More notably, at farther range from the source, the laterally traveling head wave can clearly be seen moving away from the source and continuously radiating acoustic energy back into the water column at an angle consistent with the critical angle defined by Equation 17.

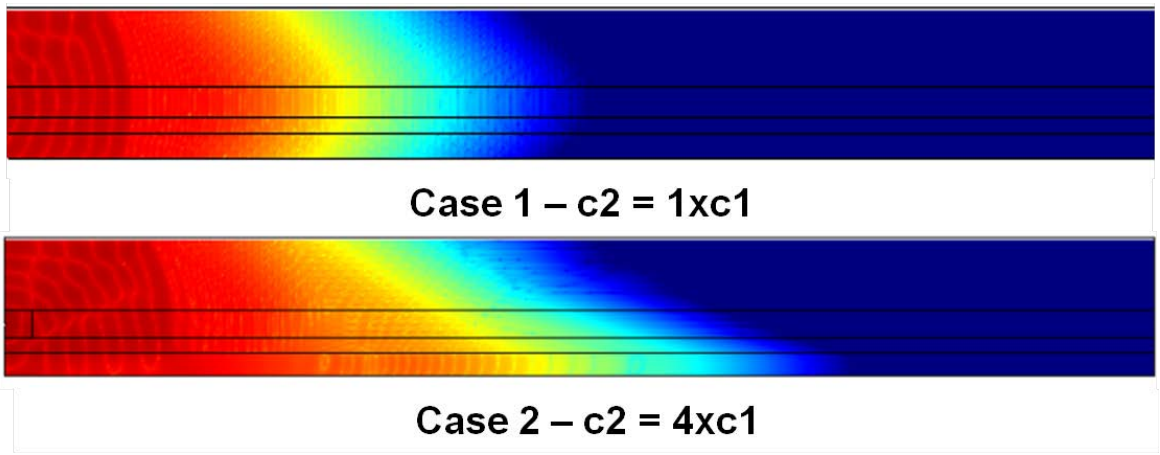

Figure 12. Comparison of the Acoustic Fields Predicted by COMSOL

For two disparate sediment sound speeds.

Additional verification of the correct prediction of the propagating head wave comes from wavenumber analysis of the acoustic field. The planar interface and material properties illustrated in Figure 3 were exercised for slightly different parameters in order to provide adequate separation of the water borne and sediment borne acoustic waves. Specifically, the densities in both media were set equal to 1000 kg/m^3 yielding a mass contrast ratio, $m \equiv \frac{\rho_1}{\rho_2}$ of 1.0. The soundspeed in the water column was set equal to 1500 m/s while the sediment was set equal to 2500 m/s, yielding an index of refraction, $n \equiv \frac{c_2}{c_1}$ of 1.66. The monopole source was located at a depth of 50 m and excited at a single

frequency of 100 Hz. All surfaces were set to be outgoing wave absorbers to mimic free-space propagation of two semi-infinite half spaces. Under such conditions, it is anticipated that there should exist two propagating wave numbers with each corresponding to the free-field motion of acoustic waves. In both the near and far fields, the water borne wave is expected to propagate radially at $k_1 = \frac{\omega}{c_1}$. Similarly, in the absence of reflection from any boundaries, the sediment wave is expected to propagate radially at $k_2 = \frac{\omega}{c_2}$. For the parameters listed above, these two wavenumbers are numerically equal to $k_1 = 0.41$ rad/m and $k_2 = 0.25$ rad/m, respectively. By sequentially extracting short segments (sliding synthetic aperture of 4096 points spaced at 1 m) of acoustic data from the pressure field, and spatially Fourier transforming them into the wavenumber domain, via Matlab's FFTW (Fastest Fourier Transform in the West) [28] Discrete Fourier Transform algorithm, it is anticipated that two distinct peaks would be observed. Presented in Figure 13 is a single sided spectrum obtained for one such virtual aperture.

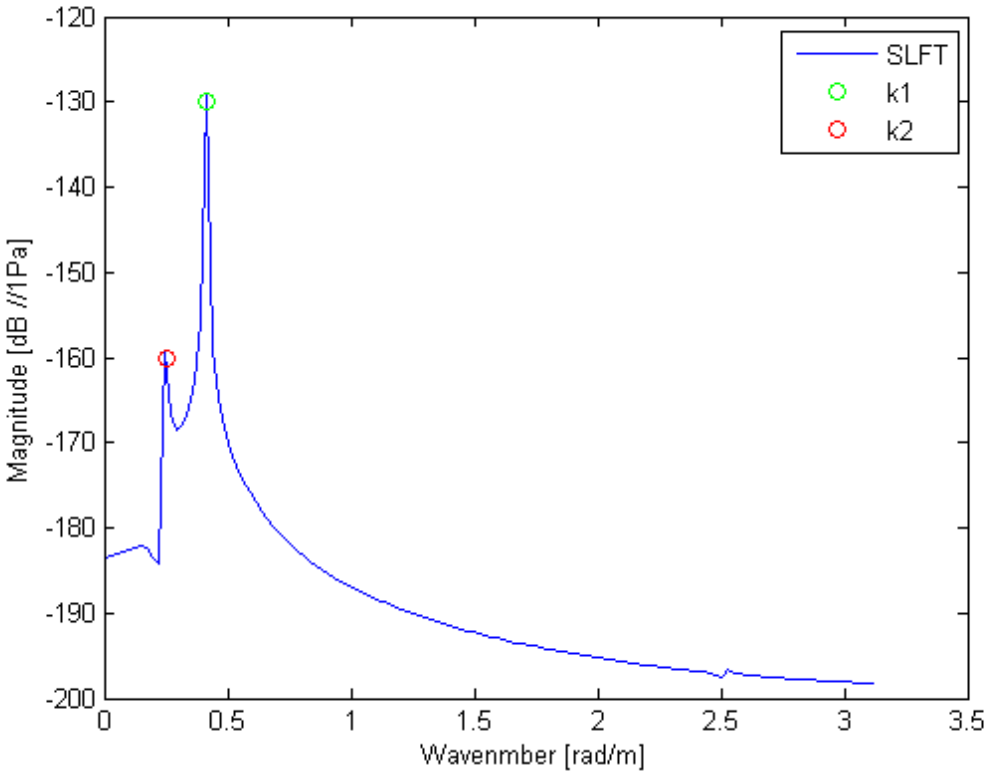

Figure 13. Single-Sided Pressure Amplitude Spectrum for Sliding Synthetic Aperture

The Short Length Fast Fourier Transformed (SLFFT) data is plotted as a continuous blue curve, with green and red circles indicating the theoretical locations of the two expected propagating wavenumbers. Of note is that the COMSOL model correctly predicts the pressure field and the relative wavenumber content. Additionally, it can be seen that the head wave propagates at a relative -30 dB with respect to the direct path. This sliding window technique allows a sufficiently long data record to accommodate fine wavenumber resolution from the windowed SLFFT. By sampling the acoustic field at dx=1 m intervals, the folding wavenumber (similar to the Nyquist limit of time domain sampling theory) is defined as $k_{fold} = 2\pi\frac{dx}{2}$, which is numerically equal to π m^{-1}. Similarly, the wavenumber resolution, which corresponds to the bin spacing of the SLFFT, is given as $\Delta k = 2\pi\frac{1}{Ndx}$. By choosing N=4096 (4096 m for the given dx sample spacing), this technique is able to resolve wavenumbers to within 0.0015 rad/m,

which is two orders of magnitude below the anticipated value of the wavenumber content.

By sequentially sliding this aperture along the length of the water-sediment interface, and stacking the resulting Fourier transformed curves (as presented in Figure 13), a wavenumber contour plot may be constructed as a function of the acoustic center of the virtual aperture. Performing this type of processing allows for an examination of the propagation length scales and amplitudes of the acoustic features present for a given bathymetry. For this simple case of two semi-infinite half spaces, it is anticipated that only two dominant wavenumbers will be present in the far field. Figure 14 shows a contour plot of the wavenumber content in this environment as a function of the location of the acoustic center of the aperture.

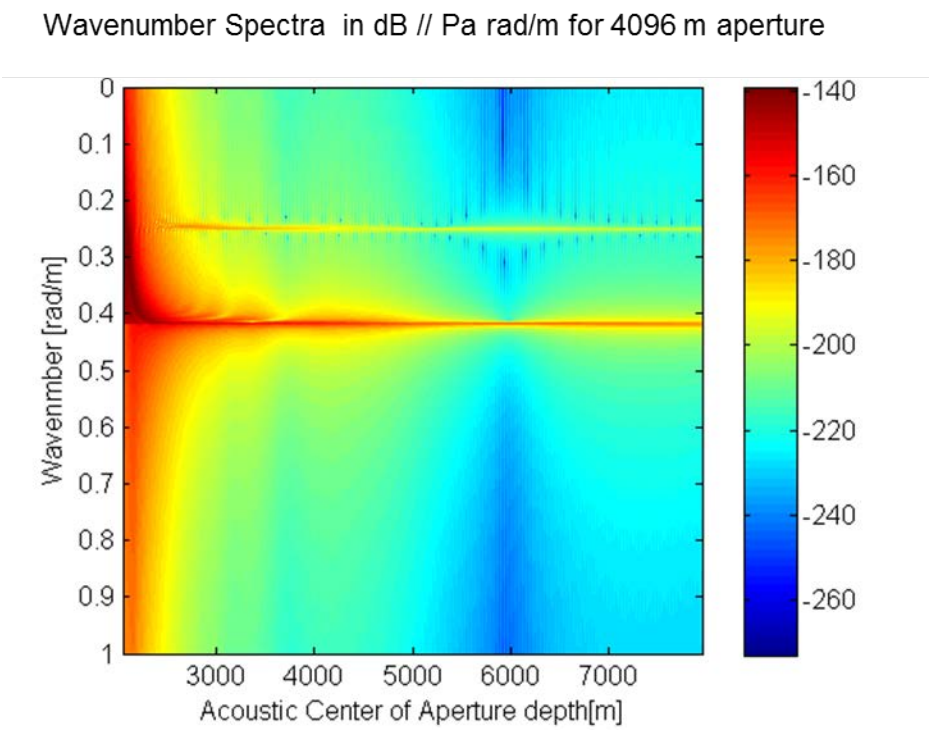

Figure 14. Wavenumber Content of the Two Semi-Infinite Half Spaces

As a function of the location of the acoustic center of the aperture.

It can be seen that in the very near field, there is still some spherical wave front curvature generated by the monopole source, resulting in curved lines on the *k-x* contour due to the size of the sliding acoustic aperture. At longer ranges, there are only two dominant wavenumbers propagating, each corresponding with theoretical predictions. This type of processing confirms the ability of COMSOL to predict the existence of the evanescent head wave.

The SLFFT processing technique also allows for a clear verification of the effects of sediment damping mechanisms. By varying the value of loss in the sediment from 0.0 to 1.0 dB/m/kHz, and examining the propagating wavenumber content in this simplified geometry, the COMSOL implementation of sediment damping may be illustrated. Presented in Figure 15 are three-color contour panels illustrating the range dependence of wavenumber for three unique damping values of 0.0, 0.1, and 1.0 stacked from top to bottom, respectively.

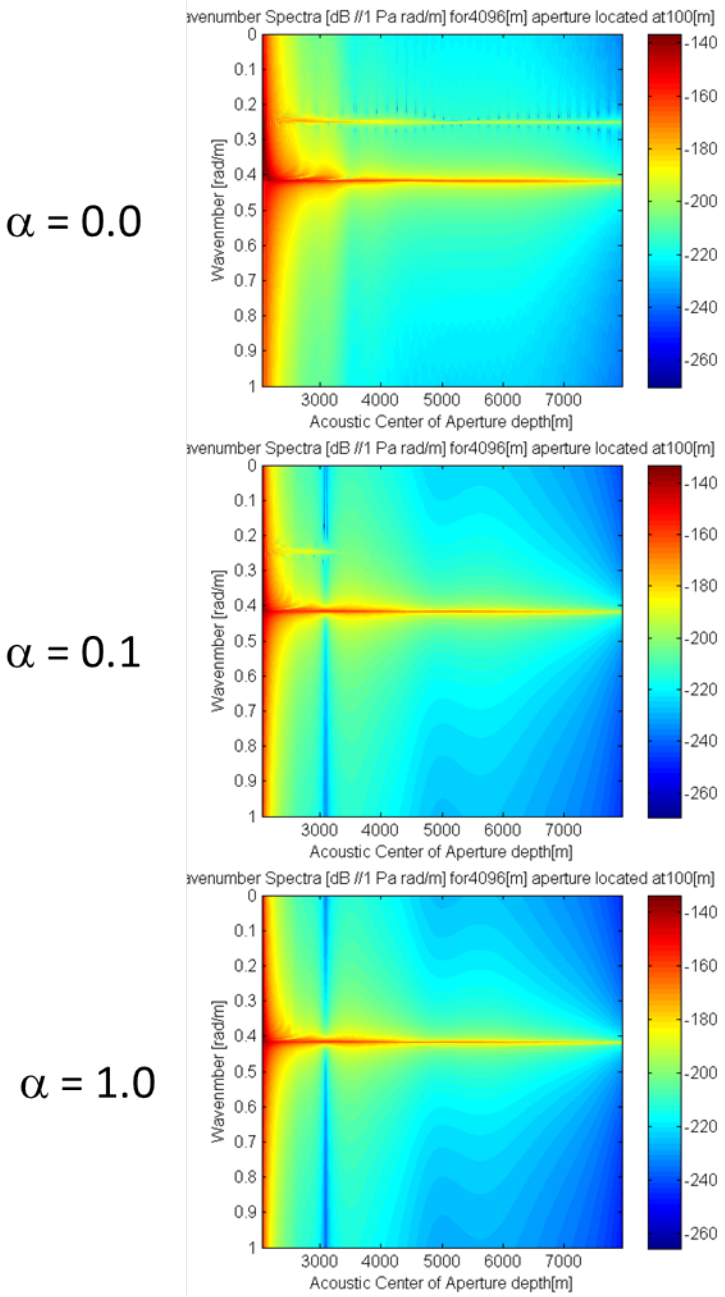

Figure 15. Range Dependence of Propagating Wavenumber Content within Semi-Infinite Half Space

In the top panel, where the sediment damping is numerically equal to zero, the lower valued wavenumber, k_2, corresponding to the sediment borne lateral wave, is consistently 30 dB less than the direct path water borne wave, and both wave types have been confirmed to experience a $\frac{1}{r^2}$ spherical spreading loss. As the sediment damping value increases to from 0 to 0.1 dB/m/kHz, it can be seen in the middle panel that the head wave starts off approximately 30 dB down relative to the direct wave. After approximately 3500 m of propagation, the head wave experiences sufficient losses such that it no longer appears in the 120 dB dynamic range of the figure. Finally, in the third panel, when the sediment damping is increased to 1.0 dB/m/kHz, the head wave contribution is damped out during the initial 1000 m of sliding aperture such that it no longer appears in the dynamic range of the plot.

D. TWO FLUID PEKERIS WAVEGUIDE

The results of the MMPE, normal modes, and COMSOL models are now compared with the inclusion of the lossless sediment bottom. Presented in Figure 16 are color contours of the magnitude of the complex valued acoustic field over the range 0–600 m from the source. It can be seen that near the source, there is reasonable qualitative agreement between the COMSOL model and the MMPE model; however, there are significant differences from the normal modes model. In the case of the COMSOL and MMPE fields, there appear to be four “finger” like structures present in the acoustic field, whereas the normal modes model does not show any particular structure. The reason for this discrepancy lies in the consideration of modes used in the summation, and will be discussed later in the analysis section of this document.

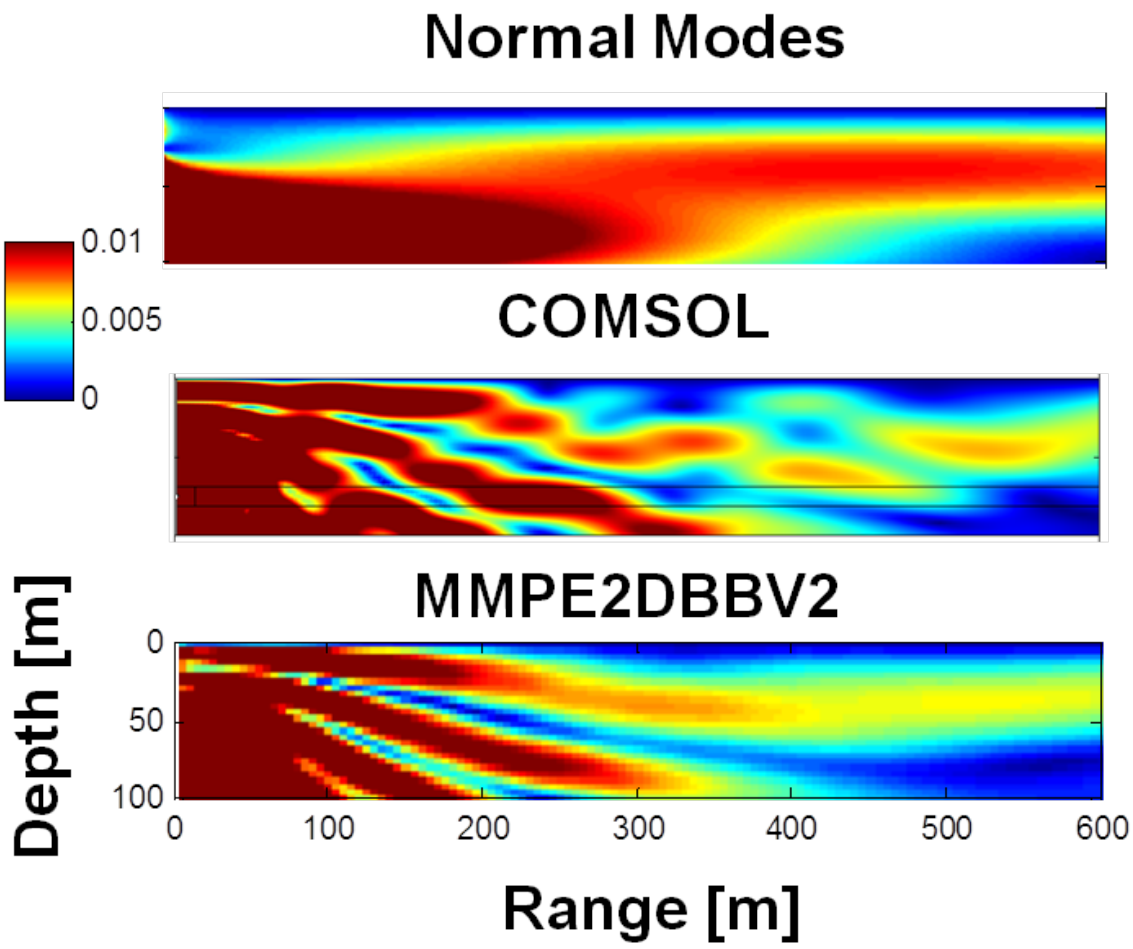

Figure 16. Comparison of Normal Modes, COMSOL and MMPE

Code predicted complex magnitude of acoustic pressure over the 0–600 m range from source with the inclusion of a lossless sediment bottom.

Presentation of the pressure field may reveal additional detail and discrepancy if the complex field is broken into its real and imaginary components and examined separately. At farther ranges, the comparison between the codes improves. Shown in Figure 17 are contours of the real component of the acoustic pressure field over the 1000–1600 m range from the source.

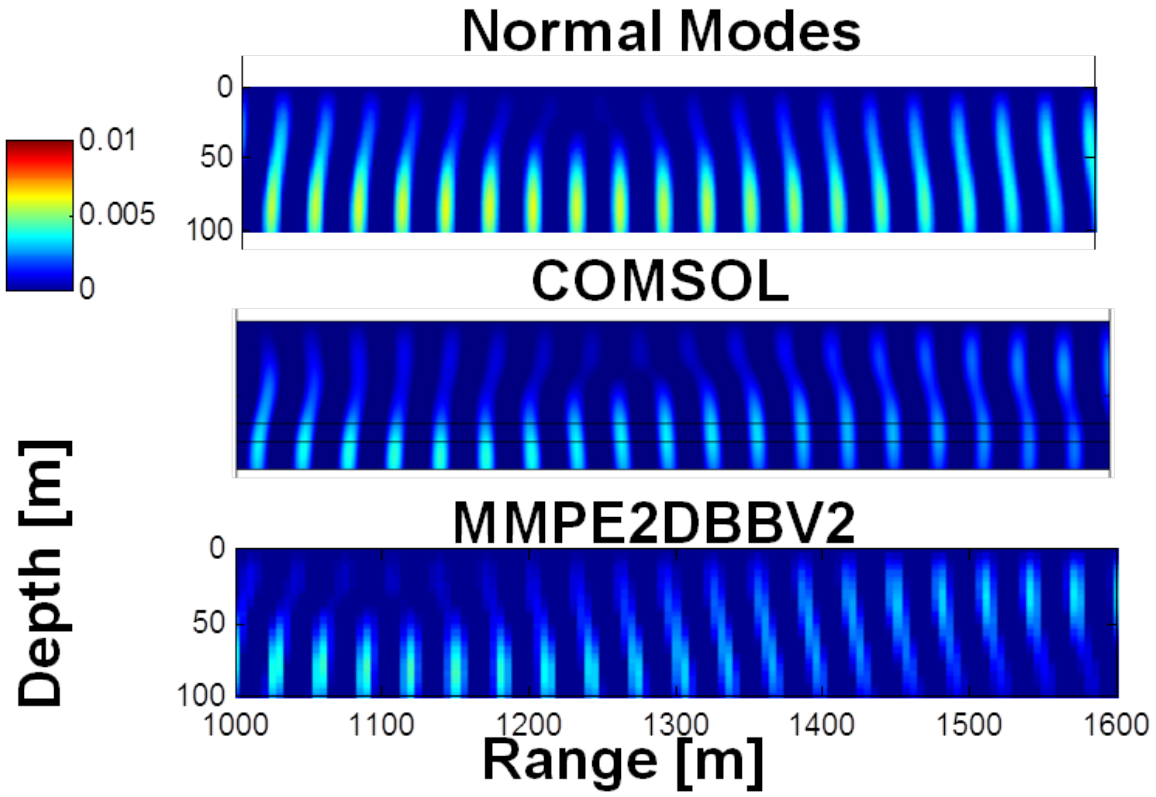

Figure 17. Comparison of Normal Modes, COMSOL and MMPE

Code predicted real component of acoustic pressure over the 0–600 m range from source with the inclusion of a lossless sediment bottom.

At these far field ranges, there is a clear pattern in the real component of pressure that is common to all three codes, indicative of the time-averaged interaction between the limited number of propagating wave fronts. It is apparent that the levels between the three methods differ slightly, with the normal modes solution having generally higher predicted values of acoustic pressure than the other two codes. However, there is a banded structure dominant in radial variation with local minima that vary in range over the 1100–1150 m range. Turning towards the acoustic intensity predicted by the three codes, there are similar trends. Presented in Figure 18 are color contour plots of the real component of the axial acoustic intensity as predicted by the three methods.

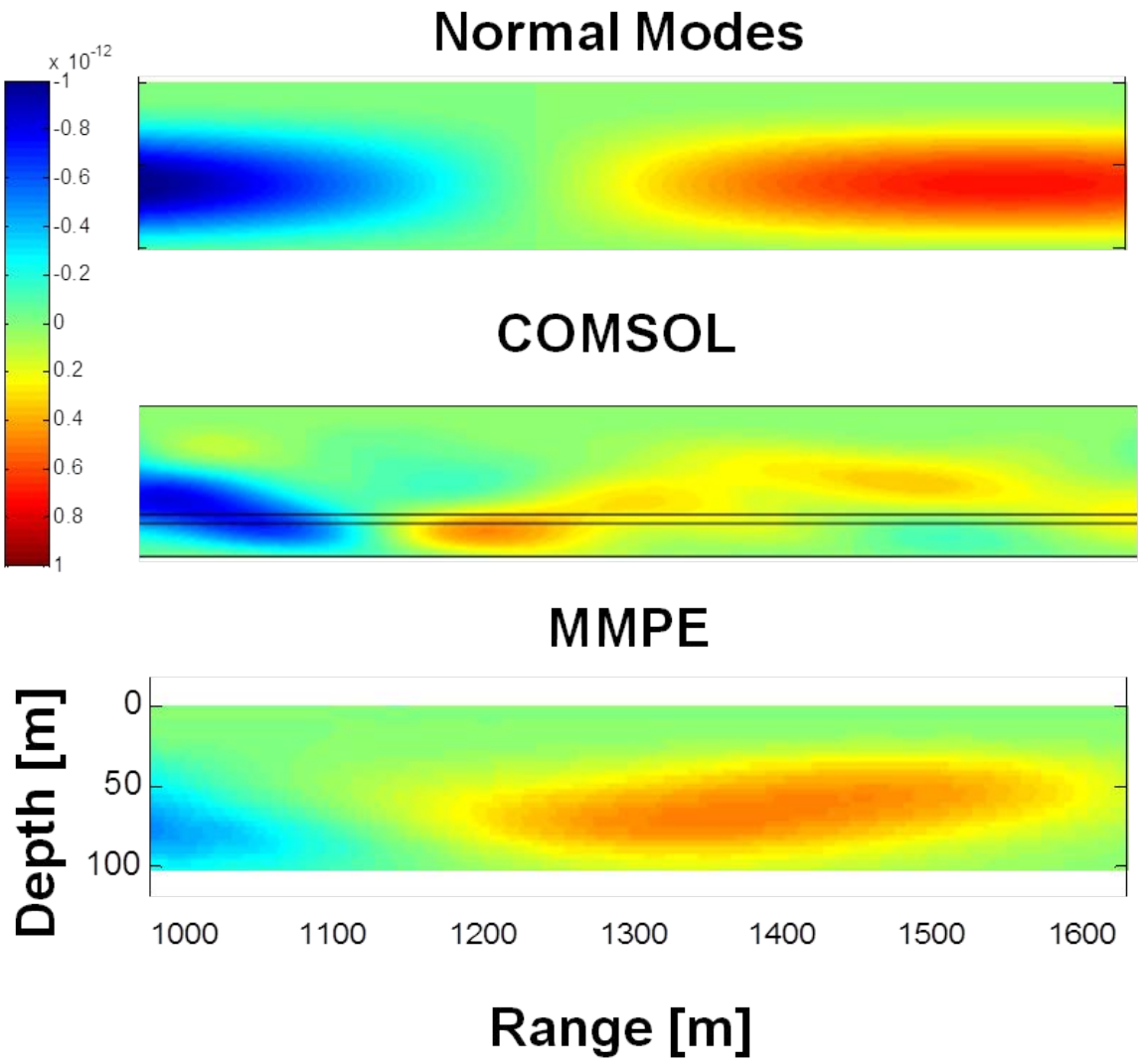

Figure 18. Contours of the Real Component of the Axial Intensity

Predicted by the three methods over a 1000–1600 m range from the source.

Here again, the normal modes method predicts slightly higher levels than the other two codes. However, the general location of regions of positive and negative intensity is in good qualitative agreement; for instance, there is a change of sign in axial intensity predicted by all methods in the 1100 to 1300 m distance from the source. Also consistent with other metrics of comparison is that COMSOL predicts significantly more structure in the intensity field than do the other two methods. The reasons will be examined in greater detail later, but this is due to the inclusion of effects of large angles of propagation.

E. UPSLOPING BATHYMETRY

Results from the up sloping environment brought out several differences between solution techniques. Discussion with NPS faculty led to the selection of an academically developed normal modes code, Couple07 [29], surmised to be capable of accurately modeling environments of this type as an alternate solver.

Couple07 is a 2007 update to the FORTRAN research code developed by Dr. Richard Evans that performs a normal mode based calculation of the pressure field. This code differs from others in that it allows for both forward and backward propagation (coupling) of modes induced by interactions with downrange bathymetric changes and range dependent sound velocity profiles.

Therefore, results from Couple 07, MMPE and COMSOL are presented to illustrate the differences in these techniques. Figure 19 shows contour plots of the active vertical intensity in the up sloping environment for a monopole source pulsating at a frequency of 20 Hz and a depth of 5 m.

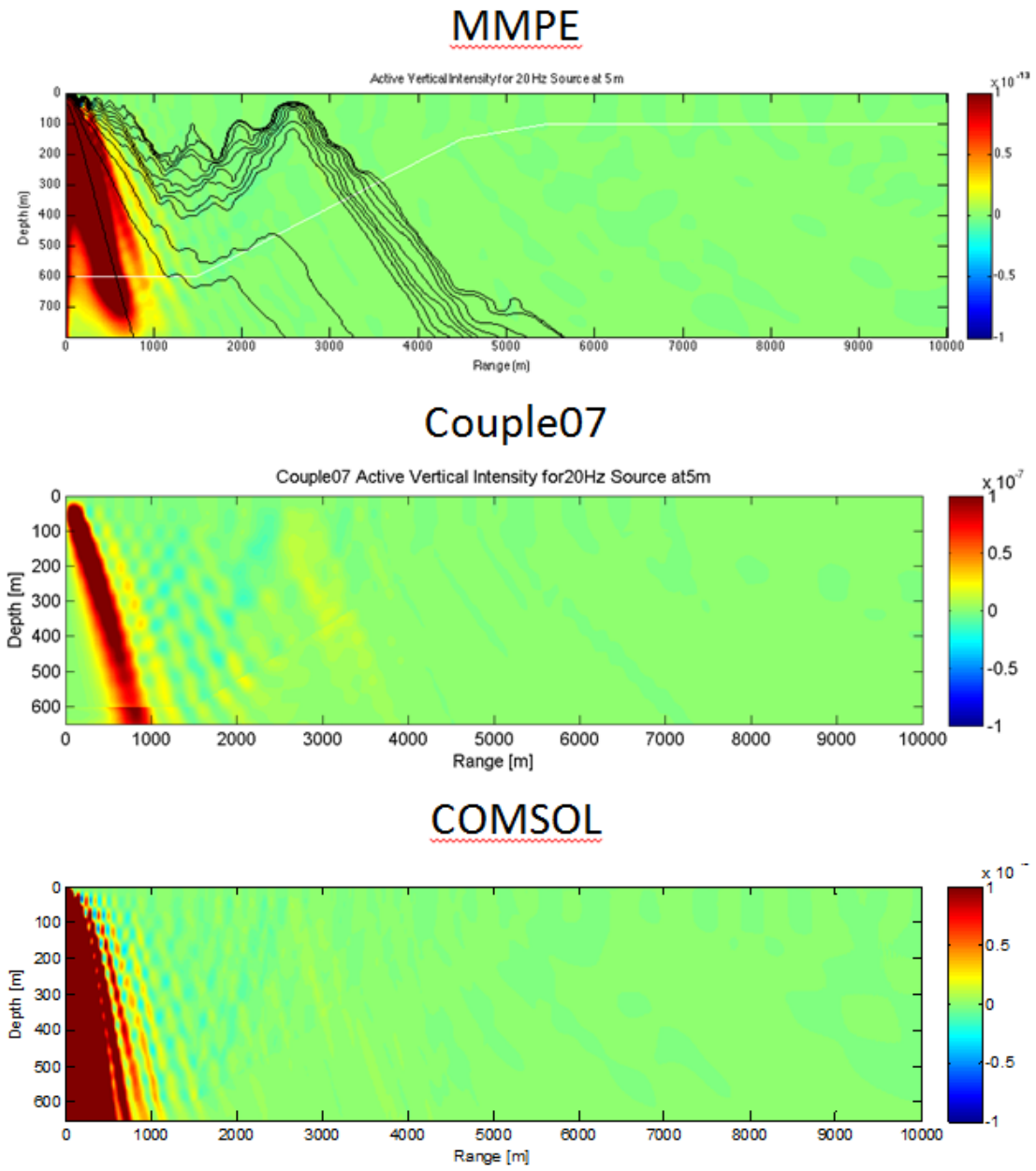

Figure 19. Comparison of MMPE, Couple 07 and COMSOL

In up sloping environment with a 20 Hz, 5 m deep monopole source.

Superimposed on the MMPE results are predicted streamlines indicating the path of energy flow in this environment. It can be seen that there is general agreement between the methods for this combination of source depth and frequency. There is measurable penetration of acoustic intensity into the sediment at a range of approximately 3500 m,

borne out by the clustering of streamlines. Increasing the frequency of excitation to 60 Hz, the field produced by COMSOL when using the background pressure field implementation shows a noticeable discrepancy from the other two techniques as shown in Figure 20. This is an anomalous prediction insofar as general agreement was found when representing the source via the specified background field, volumetric, or acceleration boundary condition.

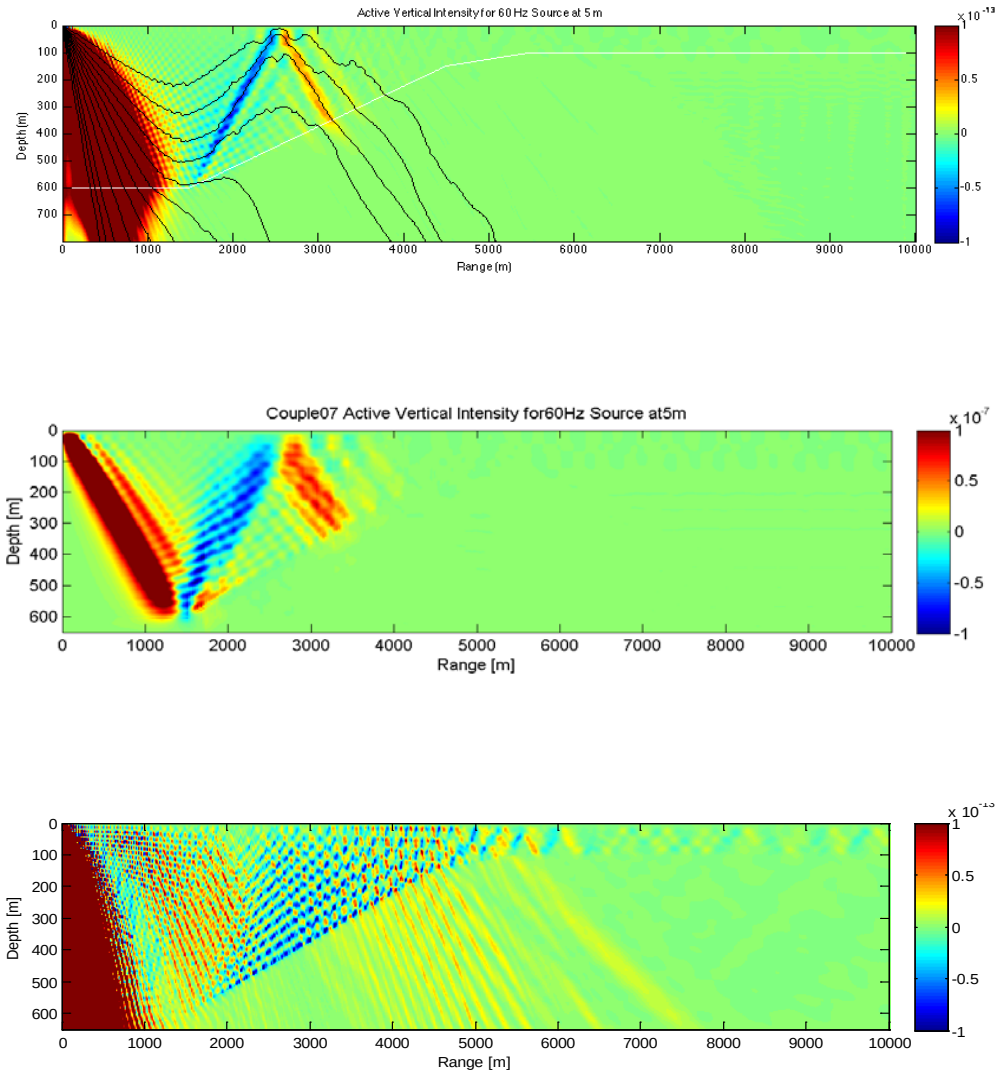

Figure 20. Comparison of MMPE, Couple 07 and COMSOL

In up sloping environment with a 60 Hz, 5 m deep monopole source.

When the source is represented instead with the acceleration-type boundary described earlier, the results from COMSOL are in much better agreement with the other two models. A contour plot of the active vertical intensity field predicted by COMSOL using both types of source models is presented in Figure 21.

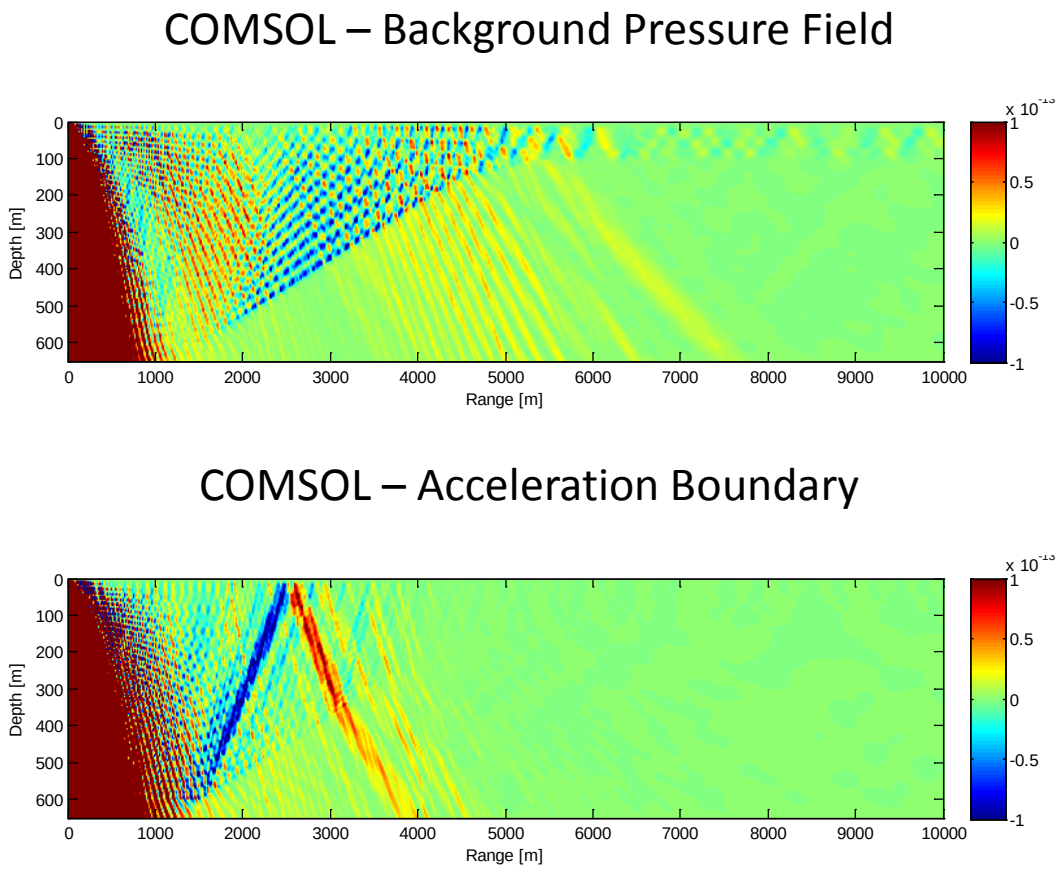

Figure 21. Comparison of the Source Model Types in COMSOL

For a 60 Hz monopole source operating at a depth of 5 m.

After discovering the sensitivity to the source type for this particular environment, it was determined that the acceleration source was the correct implementation of a monopole under such conditions due to the agreement with the other two methodologies and was thus used for the remaining modeling efforts. With this implementation of the source, several other frequency-depth combinations were studied. Presented in Figure 22

are the predictions for the up sloping bathymetry for a 60 Hz source operating at a depth of 200 m.

MMPE

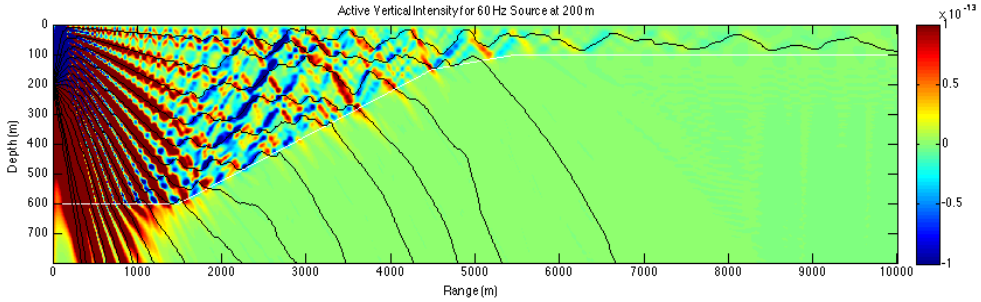

Couple07

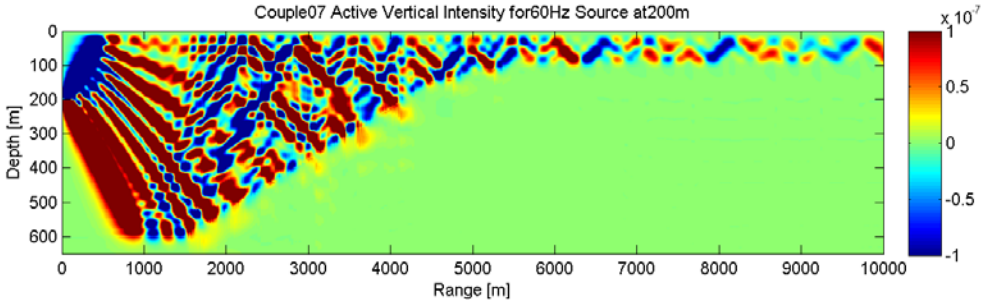

COMSOL

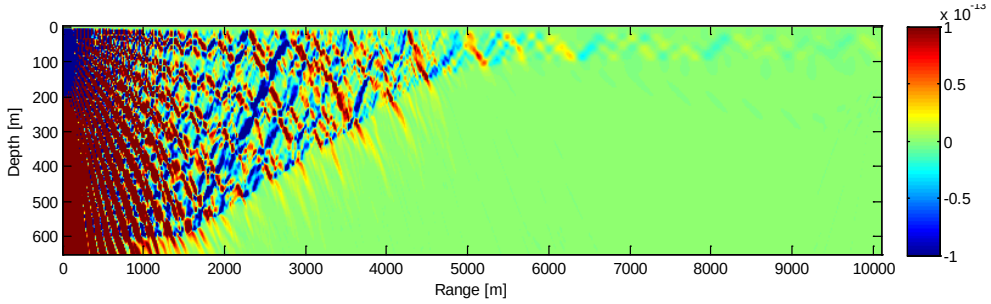

Figure 22. Comparison of MMPE, Couple 07 and COMSOL Active Vertical Intensities

In up sloping environment with a 60Hz, 200 m deep monopole source.

Again, there is excellent agreement between the three codes in both the location of regions of positive and negative intensity, and overall magnitude of the fields. Due to slight discrepancies in the scaling parameters used, it is more instructive to examine line plots of the transmission loss (TL) defined as

$$\mathrm{TL} = 20log_{10}\left(\frac{p}{p_{ref}}\right), \qquad 22$$

where $p_{ref} = 1\ \mu Pa$. Presented in Figure 23 are predictions of the transmission loss from each of the three codes as a function of range measured at 50 m from the free surface for a 60 Hz monopole source located at a depth of 200 m.

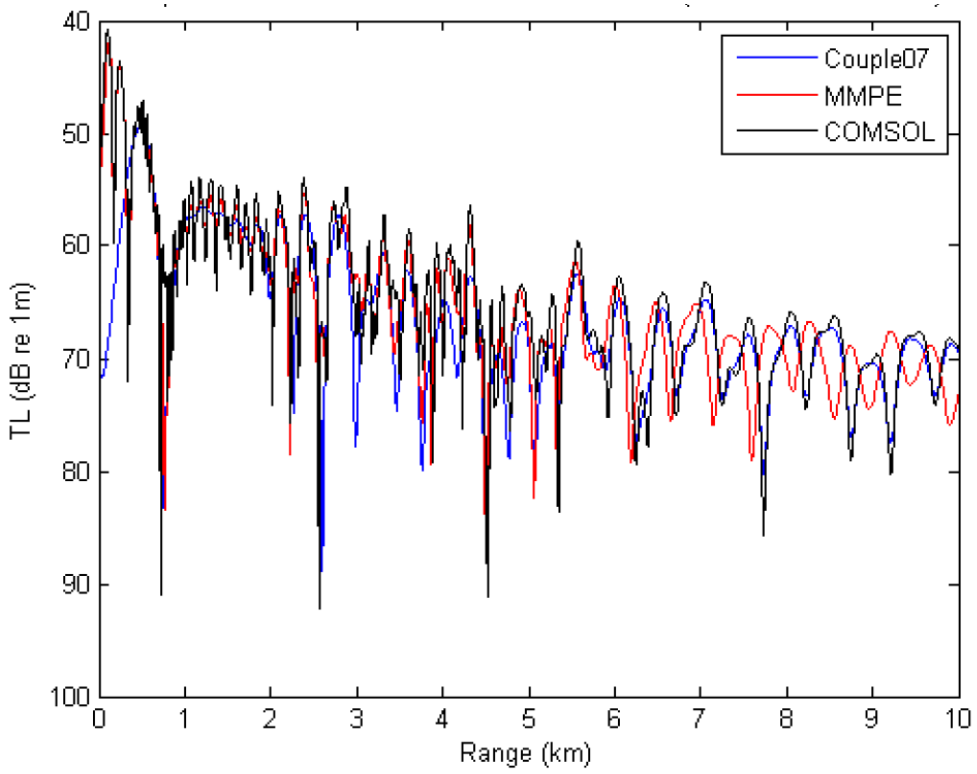

Figure 23. Transmission Loss Plotted as a Function of Range

In the up sloping environment for a 60 Hz monopole source located at a depth of 200 m.

As shown, there is excellent agreement between the three codes, with the largest discrepancy being a notable deviation in the phase predicted by MMPE, a well-

documented phenomenon, most recently described by Erdim [30]. The phase error is generated during successive forward and inverse Fourier transforms in the presence of a discontinuity between the two acoustic media. In order to prevent severe numerical difficulties several options are available, with the MMPE code making use of a density blending function. A slight (~ 2 dB) difference between the COMSOL solution and the other two techniques is attributed to the accumulated phase discrepancies.

Finally, comparisons to the results from the Smith JCA paper [11] are presented. Shown in Figure 24 is a plot of the transmission loss predicted by both COMSOL and MMPE.

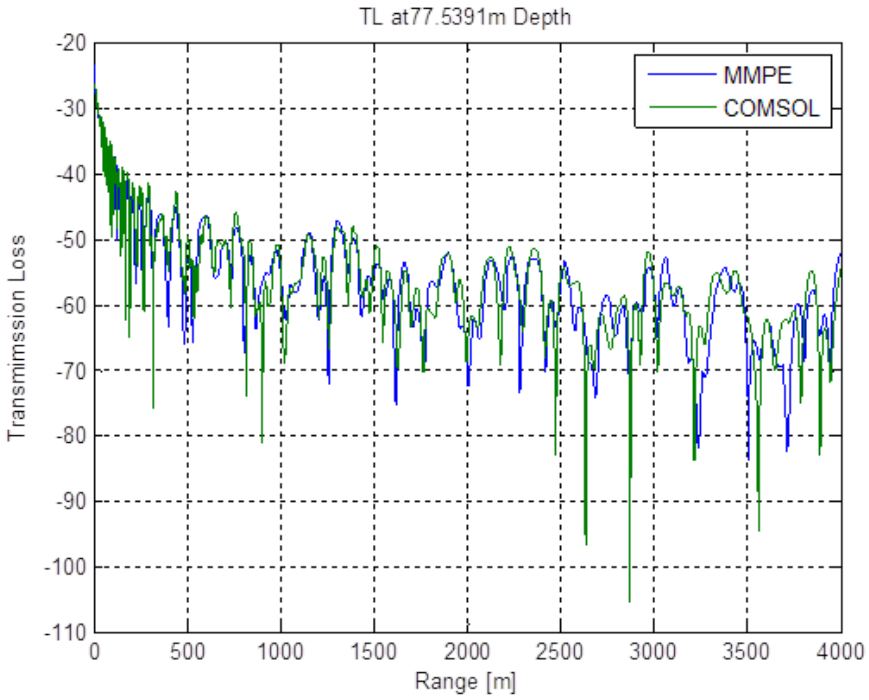

Figure 24. Comparison of the Predicted Transmission Loss from COMSOL and MMPE for the Environment Specified in JCA

It can be seen that the overall agreement between the two codes is quite good. Consistent with prior comparisons in the shallower environment, COMSOL predicts significantly more structure in the pressure field, especially at short ranges from the

source. However, the location of local minima and maxima are in good agreement, as are the overall levels with increasing range.

F. ANOMALOUS SURFACE TRANSPARENCY

Another interesting feature that can be used to investigate the accuracy of the COMSOL model was proposed by a third party reviewer and relates to the surface reflection from a true air-water interface (rather than an ideal pressure release boundary) [31]. In order to examine this effect, a model was constructed with explicit treatment of the two fluid media with both sound speed and density contrasts, *n* and *m*, respectively. By varying the vertical location of a finite sized source within the two media, several interesting phenomenon are observed.

First, it is noted that when the source is deep compared to an acoustic wavelength, the interface behaves according to classical theory (i.e., a nearly perfect reflector of acoustic energy). Specifically, when the non-dimensional source depth within the water half space, *kz*, is of order 1 or greater, most of the acoustic energy remains in the water domain. However, when *kz* drops to order 0.1 or less, most of the acoustic energy crosses the air-water boundary and becomes airborne. Presented in several panels of Figure 25 are color contours of the active vertical acoustic intensity for positive and negative (water borne and airborne) non-dimensional source depths of order 0.1 and 1.

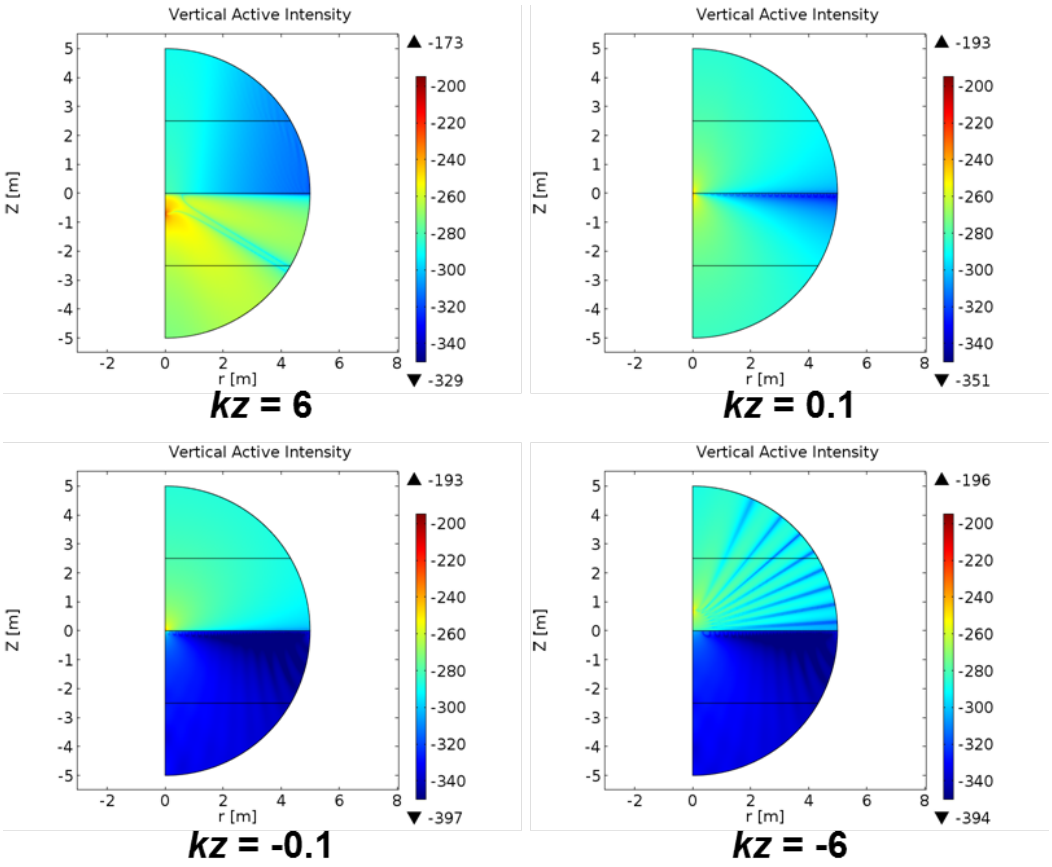

Figure 25. Contour Plots of Active Vertical Intensity for Several Source Depths

From the color contours it can be seen that not only does the majority of the acoustic energy remain in the water domain for large positive non-dimensional source depths, but what little energy is transmitted into the air remains confined to a narrow cone directly above the source. At very shallow non-dimensional source depths (order 0.1 or less), there is a sudden increase in the energy transmission, and the radiation pattern becomes increasingly omnidirectional. The relative fraction of acoustic intensity transmitted across the boundary to that reflected back into the water domain is best characterized by a quantity defined by Godin as the Transparency, T [31]. Consistent with his findings, T exhibits a fundamental asymmetry with respect to the source depth. Presented in Figure 26 is this ratio as a function of non-dimensional source depth as predicted by the theory of Godin (left) and COMSOL model results (right).

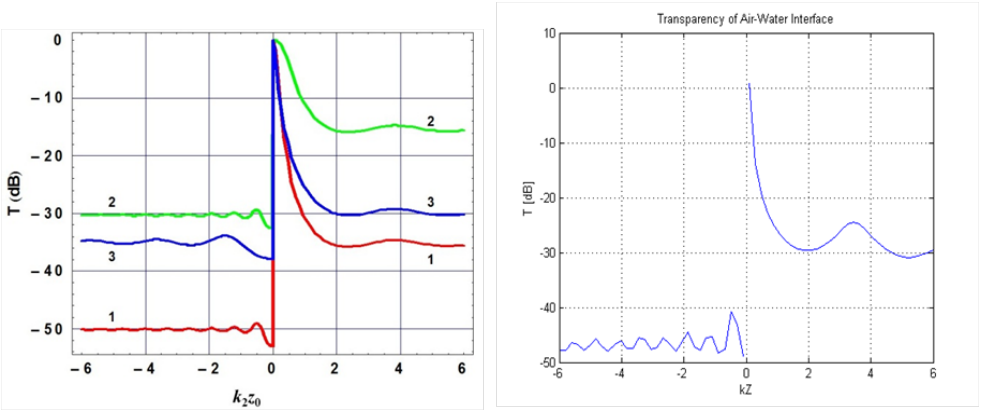

Figure 26. Acoustic Transparency of the Air-Water Interface

As predicted by Godin (left) and COMSOL (right).

While the predicted curves of Godin have been generated for several values of *n* and *m*, corresponding to the curves labeled 1–3 on the left plot, the blue curve corresponds to values typical of air and water. For these parameter values, it is noted that there is approximately a 20 dB difference between positive and negative source depths of order unity, while there is nearly a 50 dB difference for non-dimensional source depths of order 0.1 or less.

These curves serve as a point of verification that the numerical approximations of the finite element technique are solving the governing equations correctly. In addition, a point of validation, indicating that the correct equations are being solved, is desired. To that end, the model was exercised over several specific frequency-depth combinations corresponding to recent experimental work performed at the Naval Research Laboratory [32]. Figure 27 reproduced from [32], shows a schematic of the experimental setup.

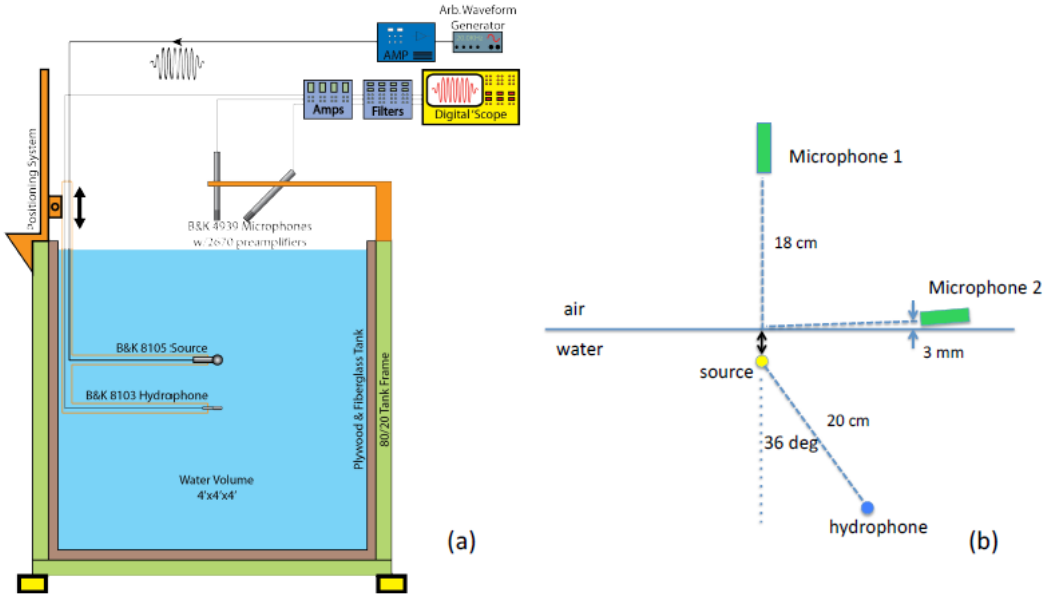

Figure 27. Schematic Diagram of the Experimental Setup Used in the NRL Experiments

Source [32]: D. C. Calvo, M. Nicholas and G. J. Orris, "Experimental verification of enhanced sound transmission from water to air at low frequencies," *Journal of the Acoustical Society of America*, vol. 134, no. 5, pp. 3403–3408, Nov. 2013.

Two airborne microphones were placed at locations on and off axis above a small spherical transducer located a small depth below the air-water interface of an acoustic test tank. A hydrophone was also located at a fixed depth relative to the source, and the relative magnitudes of the measured air and water borne pressures were recorded as functions of frequency. The ratios of these experimentally measured pressures and their theoretical predictions are compared to the values predicted by the COMSOL model in Figures 28 and 29. The figures suggest excellent agreement with the theoretical predictions. The NRL experimental data is an important verification of the theory.

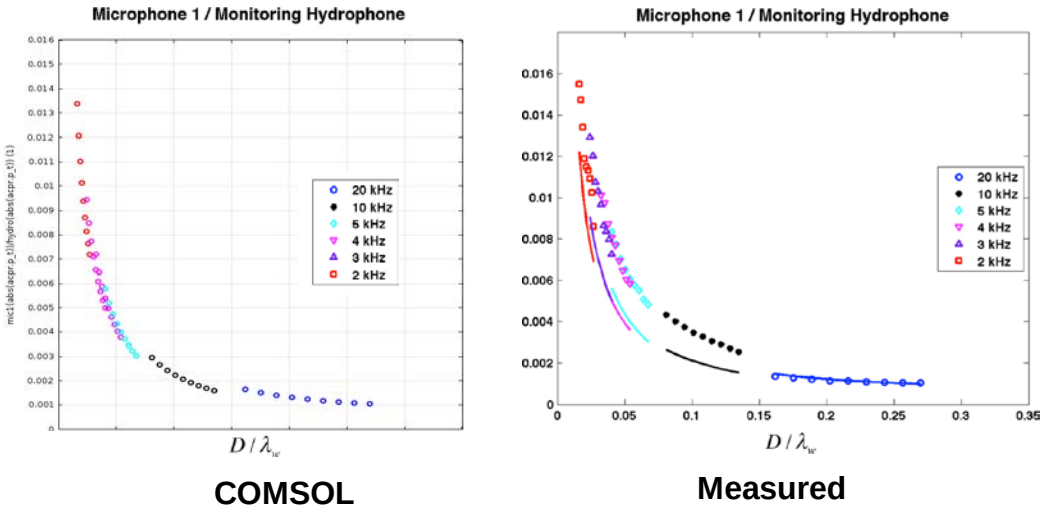

Figure 28. Comparison of the Ratios of Acoustic Pressure

In air to acoustic pressure in water plotted against non-dimensional source depth. COMSOL (Left) and NRL data (right dots) along with theoretical predictions (right lines).

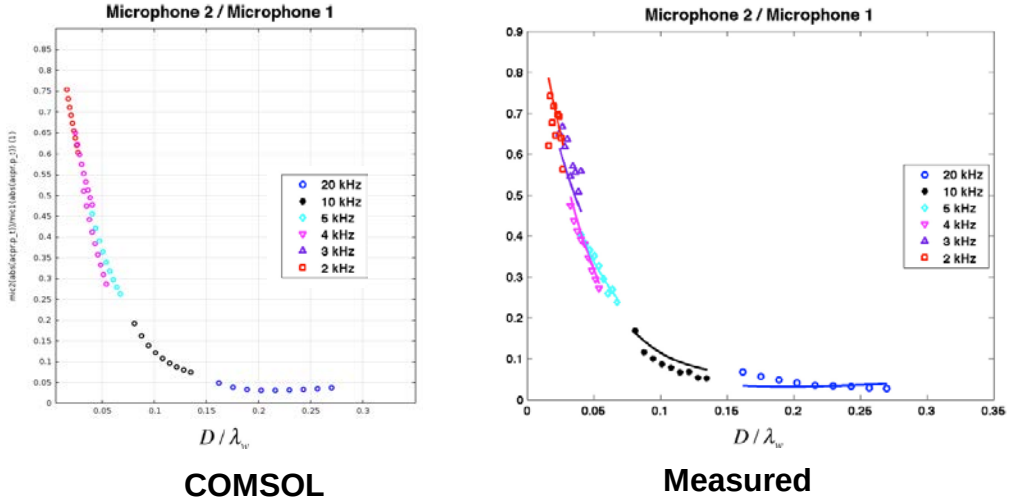

Figure 29. Comparison of the Ratios of Acoustic Pressures

Measured off-axis to those measured on-axis plotted against non-dimensional source depth. COMSOL (Left) and NRL experimental data (right dots) along with theoretical predictions (right lines).

III. ANALYSIS

Examining the plots comparing the Finite Element, Normal Modes, and Parabolic Equation methods reveals several interesting differences. First, the normal modes method consistently predicts higher levels in all fields. Second, COMSOL consistently predicts more interference patterns and features in the acoustic field than do the other two methods. Third, the PE method shows better agreement with the other two modeling approaches as both the depth of the water column and frequencies of study are increased. Finally, the trade-off between feature prediction and computational problem size is discussed.

In all cases, regardless of the treatment of the bottom interface, the normal modes based solution predicts acoustic pressure levels higher than the other two methods. Although there are no explicit material loss mechanisms present in any of the models, there are several sources of potential attenuation in both the finite element and parabolic equation approach that could account for the discrepancy in predicted pressure levels. In the finite element approach, it is well known that the density of the mesh will affect the solution. While the results presented in this work took great care to ensure adequate mesh resolution to predict an accurate field, prior efforts have indicated that levels may slightly increase in magnitude even after the heuristically determined ten linear elements per wavelength is reached. The meshes used in this study were refined to twenty quadratic elements per wavelength, and in the case of the rigid bottom, there is excellent agreement in levels between the COMSOL results and the normal mode results. The very small disparity in magnitudes between the two methods may be brought into better agreement with further mesh refinement. However, it was noted that there were no significant differences in the features predicted by COMSOL, and the sub deciBel differences were not determined to contribute to the accuracy of the solution. Therefore, this is merely a hypothesis, but is consistent with prior results.

The acoustic fields predicted by the finite element method unfailingly predict more structure and “fringing” than the other two methods. In the case of the rigid bottom, there are only slight discrepancies between the COMSOL and normal modes output. In

this case, the agreement is quite good. It is worth noting that the normal modes method does not actually propagate a solution over range, but rather seek solutions to an eigenvalue problem with the appropriate boundary conditions already enforced. This is closer to the finite element based matrix methods than is the parabolic equation approach. The results of the parabolic equation solution show large discrepancies, failing to predict nearly all of the features captured by the other two methods at any range. However, this is a well-understood limitation of the code, which is not designed for rigid bottom environments.

In the case of the sediment bottom, there is better agreement between the three methods, but COMSOL still predicts additional interference patterns. The discrepancy between COMSOL and the normal modes approach is potentially due to the presence of evanescent waves and so called “leaky” modes. The initial normal modes code has a hard limit to examine the contribution of only the trapped modes, whereas COMSOL has no such restriction. Upon switching to the coupled modes code Couple07, significantly better agreement between all three methods was observed. The discrepancies between COMSOL and MMPE are again likely due to the treatment of the bottom interface. There is a much smaller mismatch in the impedances of the two domains, however the bathymetry is still very shallow and the density mixing functions employed by this version of MMPE are likely contaminating the solution. This effect will be present at all ranges. At short ranges, it is unlikely that the two methods would exhibit good agreement due to the far-field approximations used by the parabolic equation method to generate the initial field. It is also worth noting that while both the finite element method and normal modes method seek solutions to Equation 1 (albeit through very different approaches), the parabolic method seeks solutions to a modified form of the Helmholtz equation defined in Equation 7.

As previously stated, the discrepancies between the methods when the bottom sediment is included are most likely due to the treatment of the bottom interface density discontinuity within the parabolic equation framework. When the test case documented in the JCA paper was examined, there was significantly better agreement between MMPE and COMSOL. This environment is twice as deep (200 m) and analyzed at four times the

frequency (200 Hz) with the source placed at half the depth (vice three quarters of the depth) of the water column. As such, the ratio of excitation wavelength to water column depth is much smaller than the bulk of the cases presented in this work.

The finite element approach predicts a richer feature set in the pressure field than do the normal modes and parabolic equation methods. However, the solution time and computational problem size are significantly larger when using COMSOL as compared to the other codes. Both the normal modes and MMPE executable will run on a large desktop PC (2.7 GHz 8 core Pentium with 72 GB of RAM) in well under a minute. Comparable environments require several minutes to solve within COMSOL. It is therefore important to be cognizant of the accuracy requirements of the desired numerical predictions. At higher frequencies and deeper bathymetries, the additional features predicted by the finite element method may be unwarranted due to the computing time necessary to generate them. Similarly, if the overall aim of study is to predict pressure based features, such as transmission loss alone, the accuracy afforded by parabolic equations or normal modes is likely sufficient. Here however, because of interest in the acoustic intensity field, which depends on both the pressure field and its gradient, additional time may be required to predict the necessary features accurately. This is most notable in examination of Figure 18 where the general shape and sign of the intensity field is consistent between all three methods, but there are striations predicted only by COMSOL.

The SLFT processing technique allows for a detailed examination of the propagating wave types for arbitrary bathymetries. In typical experimental data collection events, vertical line arrays (VLA) are employed in order to gain as large an aperture as possible. VLAs are also attractive due to their relative ease of deployment, naturally working in concert with Earth's gravitational field. Horizontal arrays resting along the ocean seabed are less common, but are the closest physical analog to the digital technique demonstrated herein. In either case, a long array is desired in order to provide adequate wavenumber separation during data processing. For relatively shallow water littoral environs, the depth of the water column may preclude sufficiently long aperture sizes to

examine low frequency, large wavenumber propagation. Employment of numerical models and synthetic aperture processing therefore offers several advantages.

The results of explicitly modeling the air-water interface have confirmed recently published theories regarding the transparency of said interface [32], and conditions under which classical theorems hold. In most practical applications, the product of the source depth and the wavenumber generated, *kz*, is of order unity, and classical theories describing the reflection and transmission coefficients are adequate to describe both propagating and evanescent waves [23]. However, in a limited number of cases, such as infrasonic, or very shallow source depths, the product of *kz* may drop to a value of order 0.1 or less. Under these circumstances, the mathematical treatment of Godin [33] is necessary to capture all the governing physics. COMSOL was used to verify this theory and validate against measure data.

IV. CONCLUSIONS

Three techniques have been applied to the problem of acoustic propagation in a shallow water waveguide at low frequency. For the canonical case of an ideal waveguide (pressure release and rigid boundaries), there is excellent agreement between the theory of normal modes and the finite element methods predicted using the commercial software package COMSOL. There are significant differences in the predictions of the parabolic equation based code MMPE that may be attributed to the implementation of the blending functions requisite for bottom treatment. With the inclusion of a non-rigid, sediment bottom, idealized as a second acoustic media without shear or attenuation, there is much better agreement between all three methods, though there are additional features predicted by COMSOL. This is attributed to the method by which COMSOL treats the scattering interactions from boundaries and the ability of the finite element method to capture evanescent waves. The prediction of these features comes at a significant computational cost relative to other methods, but is necessary to predict striations in the intensity field at short ranges. Further, the intensity features present in the second acoustic media are explicitly modeled. In cases where sensors lie at or below the seabed, the accuracy of the finite element method warrants the additional run-time. In many instances, these additional near-field, or sub seabed features in the intensity fields predicted by the finite element method, may not be of great importance. Under these circumstances, the PE method provides adequate resolution and allows for rapid parametric model evaluation. In cases where long range intensity features are desired, the well-known phasing issue [15] in the current MMPE code may present sufficient issues with feature prediction that a normal modes code, such as Couple07 is recommended. However, recent developments with the MMPE model have begun to mitigate this issue to improve its accuracy [34]. Furthermore, uncertainty in the knowledge of the ocean environments at long range may overwhelm such errors in practice. At exceedingly low frequencies, a full treatment of the air-water interface is necessary to capture the transmission of acoustic energy across this high-contrast boundary.

THIS PAGE INTENTIONALLY LEFT BLANK

LIST OF REFERENCES

[1] P. C. Etter, *Underwater Acoustic Modeling and Simulation*. 4th ed. Boca Raton, FL: CRC Press, 2013.

[2] K. B. Smith, M. G. Brown and F. D. Tappert, "Ray chaos in underwater acoustics," *Journal of the Acoustical Society of America*, vol. 91, pp. 1939–1949, 1992.

[3] C. L. Pekeris, "Theory of propagation of explosive sound in shallow water," *Geological Society of America, Memoir 27*, pp. 1–117, 1948.

[4] R. J. Urick, "The shallow water channel," in *Principles of Underwater Sound*. New York: McGraw-Hill, 1967, pp. 163–164.

[5] R. Kirby, "Modeling sound propagation in acoustic waveguides using a hybrid numerical method," *Journal of the Acoustical Society of America*, vol. 124, no. 4, pp. 1930–1940, 2008.

[6] E. M. Giddons and M. J. Buckingham, "On the acoustic field in a Pekeris waveguide with attenuation in the bottom half-space," *Journal of the Acoustical Society of America*, vol. 119, no. 1, pp. 123–142, Jan. 2006.

[7] J. M. Collins, H. J. Simpson and J. D. Schneiderwind, "Elastic Pekeris waveguide normal mode solution comparisons against laboratory data," *Journal of the Acoustical Society of America Express Letters*, vol. 132, no. 3, 2012.

[8] S. A. Chin-Bing and J. E. Murphy, "A finite-element model for ocean acoustic propagation and scattering," *Journal of the Acoustical Society of America*, vol. 86, no. 4, pp. 1478–1483, Oct. 1989.

[9] G. C. Diwan, S. K. Bhattacharyya and C. P. Vendhan, "Finite-element modeling of depth and range dependent acoustic propagation in oceanic waveguides," *Journal of the Acoustical Society of America*, vol. 127, no. 6, pp. 3319–3326, Jun. 2010.

[10] J. Adin Mann, J. Tichy and A. J. Romano, "Instantaneous and time-averaged energy transfer in acoustic fields," *Journal of the Acoustical Society of America*, vol. 82, no. 1, pp. 17–30, 1987.

[11] K. B. Smith, "Validating range dependent, full field models of the acoustic vector field in shallow water environments," *Journal of Computational Acoustics*, vol. 16, no. 4, pp. 471–486, Dec. 2008.

[12] D. R. Dall'Osto and P. H. Dall, "Properties of the acoustic intensity vector field in a shallow water waveguide," *Journal of the Acoustical Society of America*, vol. 131, no. 3, pp. 2023–2035, Mar. 2012.

[13] W. Duan, R. Kirby, J. Prisutova and K. V. Horoshenkov, "Measurement of complex acoustic intensity in an acoustic waveguide," *Journal of the Acoustical Society of America*, vol. 134, no. 5, pp. 3674–3685, Nov. 2013.

[14] F. D. Tappert, J. B. Keller and J. S. Papadakis, "The parabolic approximation method," in *Wave Propagation and Underwater Acoustics*. New York: Springer, 1977, pp. 224–287.

[15] K. B. Smith, "Convergence, stability and variability of shallow water acoustic predictions using a split-step Fourier parabolic equation model," *Journal of Computational Acoustics*, vol. 9, pp. 243–285, Mar. 2001.

[16] D. J. Thomson and N. R. Chapman, "A wide-angle split-step algorithm for the parabolic equation," *Journal of the Acoustical Society of America*, vol. 74, pp. 1848–1854, 1983.

[17] *The Ocean Acoustics Library*. (n.d.). Office of Naval Research. [Online]. Available: http://oalib.hlsresearch.com/PE/MMPE/. Accessed Sept. 18, 2014.

[18] F. Ihlenburg, *Finite Element Analysis of Acoustic Scattering*. New York: Springer, 1998.

[19] R. J. Barton, G. R. Moss and K. B. Smith, "Characterization of scattered acoustic intensity fields of finite cylinders in the resonance region," *Journal of the Acoustical Society of America*, vol. 130, no. 4, 2011.

[20] H. Medwin and C. S. Clay, *Acoustical Oceanography*. New York: Wiley, 1977.

[21] *MATLAB R 2010b*, , Natick, MA: Mathworks, 2014.

[22] L. Brekhovsiskh and O. Godin, *Waves in Layered Media*. Berlin: Springer-Verlag, 1978.

[23] L. Kinsler, A. Frey, A. Coppens and J. V. Sanders, *Fundamentals of Acoustics*. Hoboken, NJ: John Wiley and Sons, 2000.

[24] S. E. Crocker, T. M. Straw and R. T. Richards, "Calibration and characterization of a vector sensor towed array," *U.S. Navy Journal of Underwater Acoustics*, vol. 60, pp. 377–403, 2010.

[25] G. Floquet, "Sur les équations différentielles linéaires à coefficients périodiques," *Annales de l'École Normale Supérieure*, vol. 12, pp. 47–88, 1883.

[26] E. J. Silva and N. Ida, “A comparison of Absorbing boundary conditions to perfectly matched layers in the 2D Frequency domain finite element method,” in *Non-Linear Electromagnetic Systems*, 2000.

[27] A. Bayliss, M. Gunzburger and E. Turkel, “Boundary conditions for the numerical solution of elliptic equations in exterior regions,” *SIAM Journal of Applied Mathematics*, vol. 42, no. 2, pp. 430–451, Apr. 1982.

[28] M. Frigo and S. G. Johnson, “Design and implementation of FFTW3,” *Proceedings of the IEEE*, vol. 93, no. 2, pp. 216–231, 2005.

[29] R. B. Evans. (2011, Dec. 11). *Couple*. [Online]. Available: http://oalib.hls research.com/Modes/couple/COUPLE07.txt

[30] S. Erdim, “An Examination of higher-order treatments of boundary conditions in split-step fourier parabolic equation models,” M.S. thesis, Naval Postgraduate School, Engineering Acoustics:Monterey, CA, 2015.

[31] O. Godin, private communication, Dec. 2014.

[32] D. C. Calvo, M. Nicholas and G. J. Orris, “Experimental verification of enhanced sound transmission from water to air at low frequencies,” *Journal of the Acoustical Society of America*, vol. 134, no. 5, pp. 3403–3408, Nov. 2013.

[33] O. A. Godin, “Transmission of low-frequency sound through the water-to-air interface,” *Acoustical Physics*, vol. 53, pp. 305–312, May 2007.

[34] K. B. Smith, D. J. Thomson and P. Hursky, “An investigation into the bottom interface treatment in parabolic equation models utilizing split-step Fourier and finite-difference algorithms,” *Journal of the Acoustical Society of America*, vol. 135, p. 2430, Apr. 2014.

THIS PAGE INTENTIONALLY LEFT BLANK

INITIAL DISTRIBUTION LIST

1. Defense Technical Information Center
   Ft. Belvoir, Virginia

2. Dudley Knox Library
   Naval Postgraduate School
   Monterey, California